What is the band alignment of $Cu_2ZnSn(S,Se)_4$ solar cells?

Crovetto, Andrea; Hansen, Ole

Published in:
Solar Energy Materials and Solar Cells

Link to article, DOI:
10.1016/j.solmat.2017.05.008

Publication date:
2017

Document Version
Early version, also known as pre-print

What is the band alignment of $Cu_2ZnSn(S,Se)_4$ solar cells?

Andrea Crovetto[a,*], Ole Hansen[a,b]

[a] *DTU Nanotech, Technical University of Denmark, DK-2800 Kgs. Lyngby, Denmark*
[b] *V-SUSTAIN, Villum Center for the Science of Sustainable Fuels and Chemicals, Technical University of Denmark, DK-2800 Kgs. Lyngby, Denmark*

Abstract

The band alignment at the $Cu_2ZnSn(S,Se)_4$/CdS solar cell heterojunction is a controversial issue, as different measurements and calculations point to substantially different conduction band offsets (CBO). As the actual value of the CBO has profound implications on solar cell performance, the aim of this work is to separate genuine process-dependent variations in the CBO from errors in its experimental determination. We argue that the two most likely mechanisms responsible for real CBO variations are Fermi level pinning (which tends to decrease the CBO) and chemical interdiffusion (which tends to increase the CBO). The experimental and computational approaches employed so far to determine the band alignment are analyzed to point out possible limitations for each approach, with an emphasis on photoemission-based approaches. The influence of Fermi level pinning on the CBO should be captured correctly by all types of measurements, except for measurements performed under flat-band conditions. This may explain some particularly large values of the CBO that have been measured under flat-band conditions. On the other hand, the influence of interdiffusion is difficult to resolve completely by most measurement approaches. Interestingly, a rough correlation can be established between the CBO measured at the Cu_2ZnSnS_4/CdS interface by different groups and their corresponding solar cell efficiency: lower-efficiency cells often have a large "cliff-like" offset, whereas most high-efficiency cells have a "spike-like" or nearly flat offset. Control of interdiffusion can be a powerful way to engineer the optimal band alignment in Cu_2ZnSnS_4/CdS solar cells, but it can be detrimental in $Cu_2ZnSnSe_4$/CdS solar cells, as it may increase the CBO above the optimal range for maximum efficiency.
NOTE: IN THE PUBLISHED VERSION OF THIS ARTICLE, AN OLD VERSION OF FIGURE 3 WAS INITIALLY PUBLISHED BY THE PRODUCTION TEAM OF THE JOURNAL. THE ONE SHOWN HERE IS THE CORRECT FIGURE.

Keywords:
CZTS, kesterite, CdS, band alignment, XPS, conduction band offset

1. Introduction

The p-type semiconductor $Cu_2ZnSn(S,Se)_4$ (CZTS(e)) is among the most promising solar absorber materials on the path to thorough deployment of solar energy [1]. CZTS(e) is usually paired with an n-type CdS buffer layer to form a heterojunction solar cell. While absorbers with a high Se content (CZTSe) have achieved a promising power conversion efficiency of 12.6% at the laboratory scale [2], the record efficiency of higher-band gap absorbers with a low Se content (CZTS) lags at 9.1% [3]. In both cases, the most urgent issue to be solved is the low open circuit voltage (V_{oc}) of the solar cell compared to its theoretical maximum given by the Shockley-Queisser limit [1].

The origin of the large V_{oc} deficit, though, appears to be different in CZTSe- and CZTS solar cells. In fact, temperature-dependent V_{oc} measurements have shown that, in CZTSe solar cells of reasonable efficiency, extrapolation of the open circuit voltage to a temperature of 0 K yields a value that is just a few tens meV lower than the band gap of CZTSe [4]. As the extrapolated V_{oc} at 0 K corresponds to the activation energy of the dominant recombination path in the solar cell (E_A), it is reasonable to conclude that CZTSe solar cells are limited by bulk recombination, and that the small mismatch between V_{oc} and E_A exists because most bulk recombination occurs to/from bulk tail states [5].

Conversely, the same type of measurement done on CZTS solar cells yields values of E_A that are consistently lower than the CZTS band gap by about 0.3-0.4 eV [6–8]. This is significantly larger than the depth of tail states in CZTS, so it seems as if the dominant recombination path is not located in the CZTS bulk but at some interface instead. There can be different reasons why E_A can be lower than the absorber's band gap when interface recombination is dominant [9]. Among them, a cliff-like conduction band offset (CBO) between CZTS and its typical heterojunction partner CdS (buffer layer) is often invoked because a large fraction of the existing CBO measurements [10–26] and calculations [21, 27–33] confirms it. Here, by "cliff-like" or "negative" CBO we intend a lower-lying conduction band maximum of CdS with respect to CZTS(e) at the heterointerface, as shown in Fig. 1(b).

In a generic heterojunction solar cell with a cliff-like CBO at the heterointerface, the activation energy of interface recombination becomes equal to the energy difference between the con-

*Corresponding author, email: ancro@nanotech.dtu.dk, Ørsteds Plads, building 345 East, DK-2800 Kgs. Lyngby, Denmark, Tel.: +45 4525845

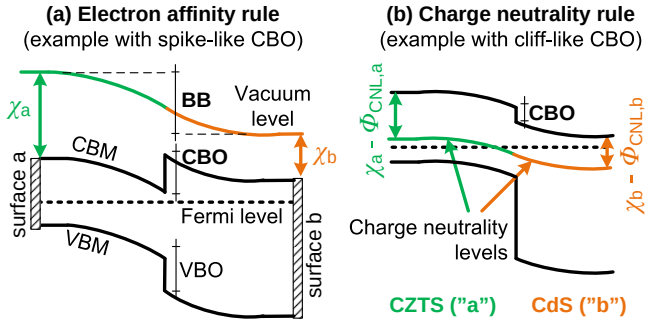

Figure 1: Band diagram showing the two limiting cases of Eq. 1 in the theoretical determination of band offsets. (a) The Schottky limit (electron affinity rule), where $S = 1$ in Eq. 1 and the materials are lined up against a common vacuum level. (b) The Bardeen limit (charge neutrality rule), where $S = 0$ in Eq. 1 and the materials are lined up against a common charge neutrality level (CNL). The qualitatively different case of a positive "spike-like" and a negative "cliff-like" CBO are shown to demonstrate the sign conventions. BB stands for band bending.

duction band minimum (CBM) of CdS and the valence band maximum (VBM) of CZTS due to cross-recombination [9]. Therefore, if interface recombination is the dominant recombination path, a cliff-like CBO will result in a lower E_A than the absorber's band gap and in a lower V_{oc}, as shown in device simulation work [27, 34, 35]. The ideal CBO for heterojunction solar cells is a moderately positive (spike-like) CBO between +0 eV and +0.4 eV [27, 34, 35] as shown in Fig. 1(a). If the spike becomes too large (>+0.4 eV) the light-generated electrons flowing from CZTS toward the top contact are blocked by the large electron barrier at the heterointerface. As will be discussed later, this problem can be encountered in (selenide) CZTSe/CdS solar cells. The valence band offset (VBO) at the heterointerface is not of primary importance as long as the band gap of the buffer is significantly larger than that of the absorber.

The above arguments may lead to the conclusion that the V_{oc} of CZTS/CdS solar cells is fundamentally limited by a cliff-like CBO. To confirm or reject this conclusion, we will try to understand the factors that determine the actual band alignment between CZTS(e) and CdS, and the factors that may lead to an incorrect measurement or calculation of the band offsets. In Sec. 2, general theory on semiconductor band alignment will be reviewed. In Sec. 3 (Sec. 4), the experimental (computational) methods employed to measure (calculate) the CBO between CZTS(e) and CdS will be discussed. In Sec. 5, previously published CBO measurements and calculations will be presented. In Secs. 6-10, different physical and chemical mechanisms that may influence the CBO will be proposed. Potential measurement errors related to those mechanisms will be discussed in parallel. Sec. 11 will present measurement issues related to sample preparation. Finally, Sec. 12 will propose how the CBO of CZTS(e)/CdS solar cells could be tuned within a certain range and Sec. 13 will summarize the most important findings of this paper.

2. Theory of band alignment of semiconductor heterojunctions

Most of the basic models of heterojunction band alignment are based on concepts developed in the 1970s and 1980s. A recent review can be found in [36]. A specific review on the band alignment of other chalcogenide semiconductors for solar cells can be found in [37]. It is now generally accepted that, in most situations, the band alignment between two ideal semiconductors is just a function of their bulk properties [36, 38–40]. By this it is intended that any contribution to the band alignment due to interfacial charge transfer can be predicted from bulk properties of the two materials without explicitly modeling the interface itself. Two interesting bulk models for the prediction of band alignment are the "electron affinity rule" (Schottky limit) and the "charge neutrality rule" (Bardeen limit). The electron affinity rule (Fig. 1(a)) aligns semiconductors based on the distance χ (electron affinity) between their conduction band and the vacuum level. The charge neutrality rule (Fig. 1(b)) aligns semiconductors based on the distance $\chi - \Phi_{CNL}$ between their conduction band and their charge neutrality level (CNL). Interestingly, those two models are simply two limiting cases of the following generalized expression for the CBO between semiconductors a and b [36].

$$\mathrm{CBO} = (\chi_a - \Phi_{CNL,a}) - (\chi_b - \Phi_{CNL,b}) - S\,(\Phi_{CNL,b} - \Phi_{CNL,a}) \quad (1)$$

The dimensionless screening parameter S ($0 \leq S \leq 1$) is a bulk property of the wider band gap semiconductor (CdS in the case of the CZTS(e)/CdS interface). S depends on the high-frequency dielectric constant ε_∞ of the material, according to an expression shown in [41]. If $S = 0$, we are in the limiting case of the charge neutrality rule and the semiconductors can be aligned against a common CNL (Fig. 1(b)). If $S = 1$, we are in the limiting case of the electron affinity rule and the semiconductors can be aligned against a common vacuum level (Fig. 1(a)). For intermediate S values, there is no universal reference level and Eq. 1 must be used instead. Taking $\varepsilon_\infty \approx 5$ for CdS [36], the above theory predicts $S \approx 0.4$ for the interface between CdS and any absorber material such as CZTS(e), $Cu(In,Ga)Se_2$ (CIGS) or CdTe. Therefore, Eq. 1 should be used instead of the electron affinity rule or the charge neutrality rule.

The charge neutrality level of CIGS has been calculated [38]. By substituting it in Eq. 1, one obtains very good agreement with experimental band offsets on CIGS/CdS interfaces without process-induced non-idealities (e.g. interdiffusion or interface defects) [37, 38, 42]. Unfortunately, the charge neutrality levels of CZTS and CZTSe have not been explicitly calculated yet and theoretical predictions of the CZTS(e)/CdS band alignment have so far been based on the computation of the full electronic structure of explicit CZTS(e)/CdS interface models. Those models will be introduced in Sec. 4.

As mentioned already, Eq. 1 is expected to be valid for "ideal" interfaces. However, a number of non-idealities can occur at real interfaces. Two widely discussed non-idealities are Fermi level pinning and interface polarization. Their influence on the band alignment of CZTS(e)/CdS solar cells will be discussed in Sec. 6 and Sec. 7 respectively. Other mechanisms

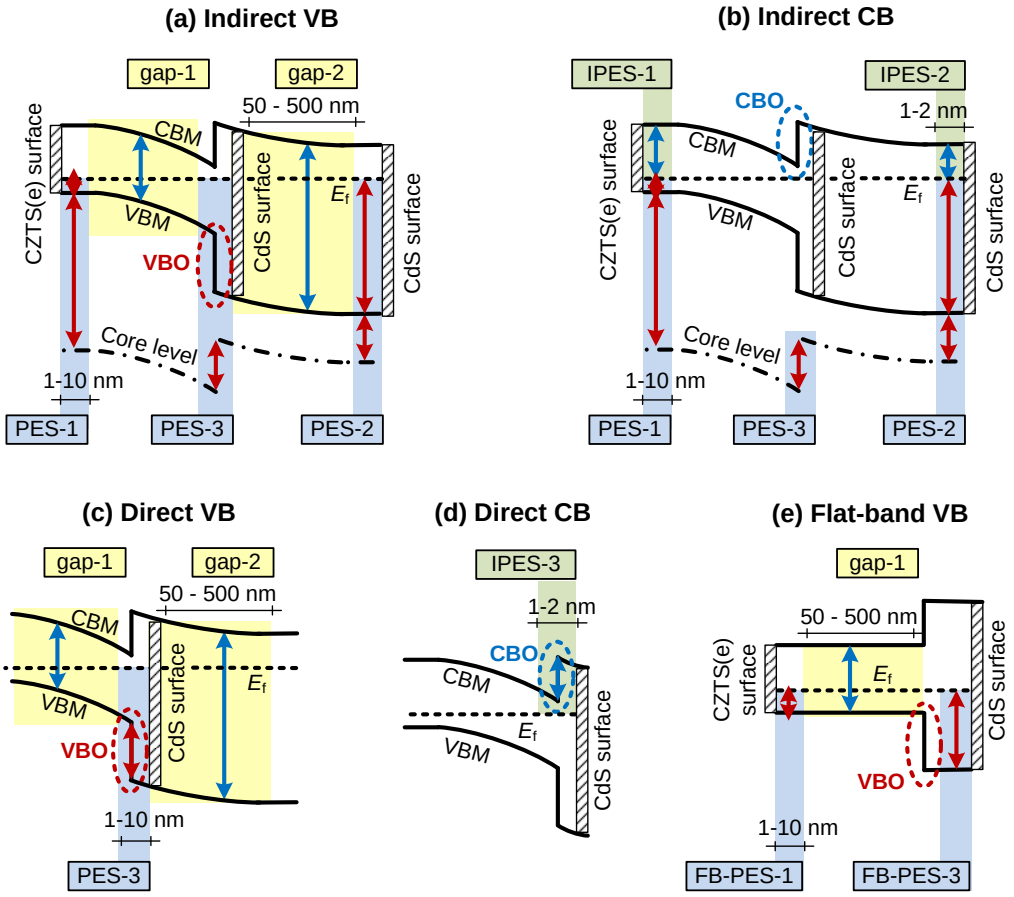

Figure 2: Sketch of the photoemission-based band alignment measurement approaches presented in Sec. 3. Blue regions: PES measurements in different regions of the device (PES-1, PES-2, PES-3, FB-PES-1, FB-PES-3). Green regions: IPES measurements in different regions of the device (IPES-1, IPES-2). Yellow regions: band gap measurements of the two bulk materials (gap-1, gap-2), typically by optical techniques. Note that the combination of a PES measurement and an IPES measurement on the same spot (for example PES-1 and IPES-1) yields the *surface* band gap of the material, due to the limited analysis depth of those techniques. Double-sided arrows: quantity measured in each measurement. Numbers: analysis depth of each measurement. Circled regions: band offset extracted by the PES or IPES technique alone, without the addition of bulk band gaps.

that may change the "ideal" band alignment involve changes in the band edge positions, band gap changes, alloying between the two materials at the interface, and formation of interface phases. Those mechanisms are not often discussed in relation to band alignment but they will be covered in this work (Secs. 8-10) as they may have a decisive role in determining the CBO of the CZTS(e)/CdS system.

3. Experimental methods

With only two exceptions [13, 16], all the CBO measurements on CZTS(e)/CdS interfaces reported so far were performed with photoemission-based techniques. Fig. 2 illustrates a number of approaches to extract the CBO by such techniques. First of all, a photoemission experiment can be of direct or inverse type. Direct photoemission spectroscopy (or simply PES) probes the density of occupied states (valence band) with respect to the Fermi level. Hence, the leading edge of the spectrum is a measure of the VBM of the material with respect to the Fermi level. PES techniques differ in terms of their analysis depth, even though they can be all considered surface-sensitive techniques. The analysis depth increases from about 1 nm to about 20 nm [43] as the wavelength of the excitation radiation decreases from ultraviolet photons (UPS), soft x-rays (XPS), to hard x-rays (HAXPES). Therefore, one must keep in mind that PES measures the valence band position close to the *surface* of the material rather than in the *bulk*, especially in the more common UPS and XPS techniques.

Opposite to direct photoemission, inverse photoemission spectroscopy (IPES) probes the density of unoccupied states (conduction band) with respect to the Fermi level. Hence, the leading edge of the spectrum is a measure of the CBM of the material with respect to the Fermi level. Since low-energy electrons are used as an excitation source, IPES is also a surface-sensitive technique (analysis depth of a couple of nm).

PES and IPES have been used to determine respectively the VBO and CBO of the CZTS(e)/CdS interface with three measurement approaches: direct, indirect, and flat-band (Fig. 2). With the indirect VB (CB) approach of Fig. 2(a,b), the distance between the VBM (CBM) and the Fermi level is mea-

sured far from the interface by PES (IPES) in both CZTS(e) and CdS. This corresponds respectively to the (I)PES-1 and (I)PES-2 measurements in Fig. 2(a,b). The VBO (CBO) at the interface is then derived by measuring band bending (BB) in the junction region, which changes the VBM and CBM positions with respect to their values away from the interface. Band bending can be extracted by XPS from a sample consisting of a thin CdS overlayer on top of CZTS(e) (PES-3 measurement in Fig. 2(a,b)). If the CdS overlayer is thinner than the analysis depth of the technique, the core levels of both materials can be resolved. By comparing the energy of the core levels in this sample to their energy away from the interface, band bending can be derived (Fig. 2(a,b)).
With the direct VB (CB) approach of Fig. 2(c,d), the valence-band (conduction-band) region of the PES (IPES) spectrum of a CZTS(e) sample with a thin CdS overlayer is deconvolved into its CZTS(e) and CdS components. This allows determination of the VBM (CBM) of the two materials directly at the heterointerface, which means that the VBO (CBO) is simply the difference between the VBM (CBM) of the two materials. See PES-3 and IPES-3 measurements in Fig. 2(c) and Fig. 2(d) respectively.

With the flat-band VB approach of Fig. 2(e), the bands of CZTS(e) are flattened by sufficiently intense optical pumping above the band gap energy of CZTS(e) but below the band gap energy of CdS. The VBO can then be obtained as the difference between the VBM position of a pure CZTS(e) sample (FB-PES-1 in Fig. 2(e)) and the VBM position of a CZTS(e) sample with a sufficiently thin CdS layer (FB-PES-3 in Fig. 2(e)) to avoid significant band bending in CdS [17].

To sum up, valence band offsets can be obtained by PES with either the indirect VB approach (Fig. 2(a)), the direct VB approach (Fig. 2(c)), or the flat-band VB approach (Fig. 2(e)). In those cases, conduction band offsets are derived by adding the bulk band gap of the two materials (gap-1 and gap-2 measurements in Fig. 2), as determined by a complementary technique such as optical transmission [22] or ellipsometry [44]. Using IPES instead, conduction band offsets can be obtained with the indirect CB approach (Fig. 2(b)) or the direct CB approach (Fig. 2(d)) without relying on separate band gap measurements.

The above approaches differ in how they approximate the band gaps of the two materials at the heterointerface:

- the three VB approaches assume that the bulk band gaps of the two materials measured by complementary techniques (gap-1 and gap-2 in Fig. 2) are equal to their band gaps at the heterointerface.

- the indirect CB approach assumes that the surface band gaps of the two materials are equal to their band gaps at the heterointerface. By "surface band gaps", the band gaps measured by the PES-1/IPES-1 measurement in CZTS(e) and by the PES-2/IPES-2 measurement in CdS in the scheme of Fig. 2(b) are intended.

- the direct CB approach does not involve any approximation for the interface band gaps because the CBO is measured directly at the heterointerface (IPES-3 measurement in Fig. 2(d)).

Therefore, any mechanism that changes the band gaps of the two materials at the heterointerface with respect to their bulk values will result in a measurement error using the VB methods. Any mechanism that changes the band gaps at the heterointerface with respect to their surface values will result in a measurement error using the indirect CB method. If the difference between the CdS band gap and the CZTS(e) band gap increases (decreases) at the heterointerface with respect to the same difference in the bulk or at surfaces, the measurement will underestimate (overestimate) the CBO.

Any of the five measurement approaches of Fig. 2 can be implemented in three ways: (i) by preparing all the necessary samples separately (a bulk CZTS(e) sample, a bulk CdS sample, and one or more CZTS samples with a CdS overlayer); (ii) by preparing a single CZTS(e)/CdS sample and gradually etching through the CdS layer by ion beam sputtering, recording photoemission spectra at different etching depths; and (iii) by growing CdS *in situ* on a CZTS surface and recording photoemission spectra at different stages of film growth.

For completeness, we briefly mention the non-photoemission based techniques used to measure the CZTS(e)/CdS band alignment in the two remaining cases [13, 16]. The first is near-edge x-ray absorption fine structure (NEXAFS), which is an alternative technique to IPES for measuring the CBM position and therefore is an alternative indirect CB approach [13]. The second technique is the electrochemical measurement, from which the flat-band VBM of a single bulk material can be determined with respect to the potential of a reference electrode [16].

4. Computational methods

Methods to obtain valence- and conduction band offsets (VBO and CBO) from first principles have been recently reviewed [45]. Among them, an explicit interface modeling method inspired by the photoemission measurement has gained significant popularity due to its excellent agreement with experimental data [46–48]. In this method, the energy positions of the valence bands of CZTS(e) and CdS are first calculated separately in the two unstrained bulk materials with respect to a reference energy unique to each bulk calculation (for example, the position of a core level). Then, an explicit model of the interface is built, where CdS is artificially strained to match the lattice constant of CZTS(e). Lattice-matching is necessary to keep the size of the interface region (which must be periodic in the interface plane) small enough so that its electronic structure can be calculated within a reasonable time. Once the interface electronic structure is calculated, the two previously determined valence band positions can be aligned against a common energy reference, typically a core level just like in the (experimental) indirect VB approach described in Sec. 3 and Fig. 2(a). Most of the existing computational studies on the CZTS(e)/CdS interface employ this method. An exception is the method employed in Refs. [27, 33], where the CBO is determined directly by inspection of the calculated band edge positions at the interface. This is made possible by performing the calculation over

a deeper interface region and by simulating an applied voltage to obtain flat band conditions. Under such conditions it is possible to separate the band edges from interface-induced states, which prevents direct evaluation of band offsets in other computational methods. This approach is conceptually similar to the (experimental) direct VB approach described in Sec. 3 and Fig. 2(c).

Even though many important computational details differ in each study, all those theoretical investigations can be broadly divided into two categories. In the first category [27, 30, 33] the goal is to model a real epitaxial (i.e., strained) interface. This means that the band gap of CdS in the interface region can be different from that in the bulk due to the slightly deformed lattice. This class of models allows for interface band gap changes. In the second category [28, 29], even though CdS is still strained in the calculation to match the lattice constant of CZTS, the effect of strain on the electronic structure is subtracted later by using a volume deformation potential correction [48]. Therefore, this second category of studies calculates the band alignment of unstrained interfaces assuming that no band gap changes occur at the interface. With other words, it models a non-epitaxial interface. This is sometimes called the "natural" band alignment [46] and it can be directly compared to the prediction of Eq. 1 based on bulk theories. It implies that band offsets are transitive, so that all semiconductors can be lined up in a single diagram with a common energy reference.
The remaining studies [21, 31, 32] employ a more approximate approach as they neither allow the interface gap of CdS to vary with respect to its bulk band gap, nor do they add a volume deformation potential correction.

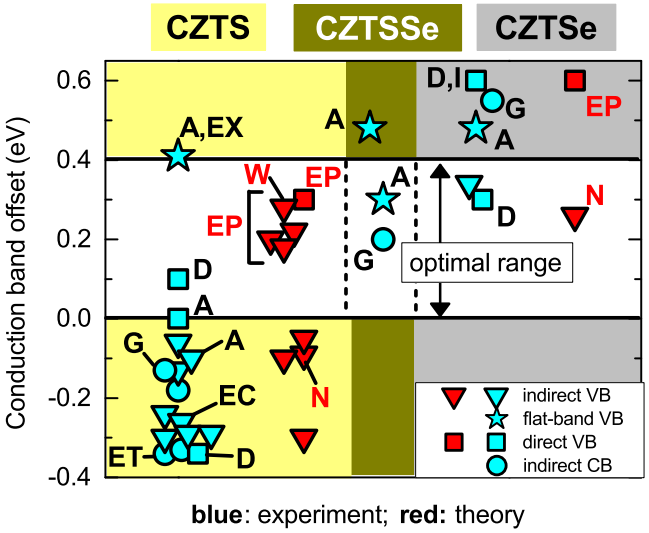

Figure 3: CBO of CZTS/CdS-, CZTSSe/CdS-, and CZTSe/CdS interfaces as determined in experimental work (blue symbols) and theoretical work (red symbols). More details for each data point are available in Table 1 and Table 2. The different symbols refer to the different measurement approaches of Fig. 2, which can also be used to describe the computational approaches as discussed in Sec. 4. **D**: depth-dependent measurement performed by progressively etching a CdS/CZTS(e) sample with an ion beam and recording PES spectra at different etching stages. **I**: abnormal interdiffusion identified in the study. **ET**: absorber etched by KCN before CdS deposition. **EC**: electrochemical measurement. **G**: *in situ* measurement taken by recording photoemission spectra during growth of CdS by evaporation on CZTS(e). **A**: CZTS(e)/CdS interface annealed before the band alignment measurement. Annealing conditions: 150-170° in ultra-high vacuum for 5 s [17, 25] and 200° in N_2 for 20 min [6, 24]. **EX**: non-straightforward extrapolation of the leading edge of the photoemission spectrum, which may increase the error bar of the measurement. See Sec. 8.1.2. **W**: calculation performed with wurtzite CdS instead of zincblende CdS. **EP**: modeling of an epitaxial interface where the band gap of CdS is allowed to vary at the heterointerface. **N**: modeling of the "natural" band alignment of a non-epitaxial (unstrained) interface.

5. Review of band alignment between CZTS(e) and CdS

A summary of all previous work on band alignment of the CZTS(e)/CdS interface known to the authors is provided in Fig. 3, Table 1, and Table 2. The following general trends can be observed:

1. The CZTSe/CdS interface has a larger CBO than the CZTS/CdS interface.
2. The CBO of the CZTS/CdS interface determined experimentally with the flat-band VB approach is an outlier. The measured value is much larger than in all other experimental reports.
3. There is a significant deviation in the reported CBO values, especially at the CZTS/CdS interface (note that there exist about three times as many studies on CZTS/CdS than on CZTSe/CdS).

In the next sections, we will examine the above points one by one by analyzing the existing band alignment studies.

5.1. Larger conduction band offset for CZTSe than for CZTS

This is qualitatively consistent with theory and can be explained by the nature of the VBM and CBM of CZTS(e). The CBM consists mostly of the antibonding state of Sn *s* and S(Se) *s* orbitals. The VBM consists mostly of an antibonding state from Cu *d* and S(Se) *p* orbital hybridization [29, 52]. The *s* and *p* orbitals of S are at a lower energy than the corresponding Se orbitals, which tends to shift the bands of CZTS to a lower energy than in CZTSe. However, the Cu-S and Sn-S bonds are shorter than the Cu-Se and Sn-Se bonds respectively, which increases level repulsion and tends to shift the bands of CZTS to a higher energy than in CZTSe. First-principles calculations can elucidate which of the two tendencies dominates at each band edge [29]. In the valence band, the down-shift tendency is stronger, so the valence band is expected to lie at a lower energy in CZTS than in CZTSe. Conversely, in the conduction band the up-shift tendency is stronger, so the conduction band is expected to lie at a higher energy in CZTS than in CZTSe [29]. From this theoretical argument, the CBO of the CZTS/CdS interface is expected to be lower than the CBO of the CZTSe/CdS interface in the absence of non-idealities such as Fermi level pinning or interface polarization. However, the difference between the CBOs of the two material pairs is expected to be *smaller* than the difference in band gap between CZTS and CZTSe (0.5 eV) due to the valence band down-shift in CZTS. Indeed, the difference in CBO for the two material pairs was found to be 0.35 eV and 0.4 eV in two independent

Publication	S/(S+Se)	Method	CBO (eV)	BB (eV)	Technique	Notes	η (%)	V_{oc} (mV)	J_{sc} (mA/cm^2)	FF (%)
Li et al. [14]	1 (CZTS)	indirect VB	−0.06		XPS					
Santoni et al. [15]	1 (CZTS)	indirect VB	−0.30	+0.14	XPS	**D**	3.2	581	11.1	49.4
Yan et al. [13]	1 (CZTS)	indirect VB	−0.24	+0.12	XPS		1.5	470	8.9	35.7
Dong et al. [21]	1 (CZTS)	indirect VB	−0.13		XPS					
Chen et al. [23]	1 (CZTS)	indirect VB	−0.28		XPS					
	1 (CZTS)	indirect VB	−0.29		UPS					
Than Htay et al. [22]	1 (CZTS)	indirect VB	−0.29		XPS		4.5	632	14.6	48.7
Kataoka et al. [24]	1 (CZTS)	indirect VB	−0.1	−0.03	HAXPES	**A**	9.1	701	20.8	62.5
Santoni et al. [15]	1 (CZTS)	direct VB	−0.34		XPS	**D**	3.2	581	11.1	49.4
Tajima et al. [11]	1 (CZTS)	direct VB	+0.0	+0.0*	HAXPES	**A**	7.1	630	18.8	60
Kato et al. [19]	1 (CZTS)	direct VB	+0.1	+0.2*	UPS	**D**	8.8	706	20.7	60.5
Terada et al. [12]	1 (CZTS)	indirect CB	−0.13		IPES	**G**	8			
Yan et al. [13]	1 (CZTS)	indirect CB	−0.18		NEXAFS		1.5	470	8.9	35.7
Bär et al. [10]	1 (CZTS)	indirect CB	−0.33	−0.10	IPES		4.1	541	13.0	59.8
	1 (CZTS)	indirect CB	−0.34	+0.14	IPES	**E**	4.1	541	13.0	59.8
Haight et al. [17]	1 (CZTS)	flat-band VB	+0.41	+0.29	UPS	**A,EX**	8.4	661	19.5	65.8
Huang et al. [16]	1 (CZTS)	other	−0.26		electrochem.	**EC**				
Terada et al. [12]	0.28	indirect CB	+0.2		IPES	**G**	10			
Haight et al. [17]	0.45	flat-band VB	+0.48	+0.12	UPS	**A**	9.7	516	28.6	65
Sardashti et al. [25]	0.3	flat-band VB	+0.3		UPS	**A**	11	480	34	68
Li et al. [18]	0 (CZTSe)	indirect VB	+0.34		XPS					
Kato et al. [19]	0 (CZTSe)	direct VB	+0.3	+0.2*	UPS	**D**	10.8	502	33.5	64
Kato et al. [19]	0 (CZTSe)	direct VB	+0.6		UPS	**D, I**	5.4	494	33.5	32.7
Haight et al. [17]	0 (CZTSe)	flat-band VB	+0.48	+0.28	UPS	**A**	9.3	412	36.4	62
Udaka et al. [26]	0 (CZTSe)	indirect CB	+0.55	+0.65	IPES	**G**	7.2			

Table 1: Compilation of CBO measurements of the CZTS(e)/CdS interface. Band bending (BB) is not always mentioned explicitly in the referenced works, but it can be derived if core level positions are provided by the authors. When the * symbol is present, band bending does not include the (long-range) electrostatic band bending due to the doping difference between CZTS and CdS but only (short range) band bending over a region of roughly 10-20 nm. The four columns on the right quote the efficiency η, open circuit voltage V_{oc}, short circuit current J_{sc}, and fill factor FF of the resulting solar cells. The sources of solar cell data are either the reference article given in the corresponding table row or one of the additional references listed in the caption of Fig. 4. See caption of Fig. 3 for a key to the abbreviations used in the Notes column.

Publication	S/(S+Se)	Method	CBO (eV)	Approach (bulk)	Approach (interface)	Interface type	Interface orientation	Notes
Chen et al. [28]	1 (CZTS)	indirect VB	−0.06	GGA	GGA	natural	(001)/(001)	**N**
Nagoya et al. [30]	1 (CZTS)	indirect VB	+0.18	HSE	GGA	epitaxial	(100)/(100)	**EP**
	1 (CZTS)	indirect VB	+0.20	HSE	GGA	epitaxial	(112)/(111)	**EP**
	1 (CZTS)	indirect VB	+0.22	HSE	GGA	epitaxial	(102)/(101)	**EP**
	1 (CZTS)	indirect VB	+0.28	HSE	GGA	epitaxial	(112)/(0001)	**W, EP**
Bao et al. [32]	1 (CZTS)	indirect VB	−0.1	GGA	GGA	undefined	(100)/(100)	
	1 (CZTS)	indirect VB	−0.3	GGA	GGA	undefined	(001)/(001)	
Dong et al. [21]	1 (CZTS)	indirect VB	−0.05	HSE	GGA	undefined	(001)/(111)	
Crovetto et al. [33]	1 (CZTS)	direct VB	+0.3	GGA+U	GGA+U	epitaxial	(100)/(100)	**EP**
Chen et al. [29]	0 (CZTSe)	indirect VB	−0.09	GGA	GGA	natural	(001)/(001)	**N**
Palsgaard et al. [27]	0 (CZTSe)	direct VB	+0.6	GGA+U	GGA+U	epitaxial	(100)/(100)	**EP**

Table 2: Compilation of first-principles CBO calculations of the CZTS(e)/CdS interface. GGA: generalized gradient approximation [49]. GGA+U: generalized gradient approximation with an added empirical U parameter to match the experimental band gap of the materials [50]. HSE: hybrid functionals by Heyd, Scuseria and Ernzerhof [51]. The "interface orientation" column gives the orientation of the CZTS(e) interface plane followed by the orientation of the CdS interface plane. See caption of Fig. 3 for an explanation of the notes.

computational studies [29, 33].

This leads to a first inconsistency: a large fraction of experimental studies on CZTS/CdS reports a CBO < -0.2 eV, and all experimental studies on CZTSe/CdS report a CBO $\geq +0.3$ eV (Fig. 3 and Table 1). The difference between the two sets of CBOs is indeed larger than the band gap difference (0.5 eV). As this contrasts with theory, it is likely that the experimental band alignment depends on some non-idealities in the materials

or at the interface, or that it is affected by measurement errors. In the next sections we will examine such possibilities.

5.2. *Larger conduction band offset with the flat-band VB approach*

In the experiment reported in [17], flat-band conditions were obtained by performing a UPS measurement under optical pumping. The photon energy of the optical excitation was below the CdS band gap but above the CZTS(e) band gap, which resulted in an excess carrier population in CZTS(e). In this way, the built-in electric field of the p-n junction on the CZTS(e) side is screened by the excess free carriers as long as the the intensity of the optical pump is high enough. Consequently, the bands on the CZTS(e) side of the junction flatten, as shown in [53] and in Fig. 2(e). The thickness of the CdS layer in the experiment in [17] was kept to a minimum in order to obtain approximately flat bands on the CdS side as well. As long as the bands are flat, Fig. 2(e) demonstrates that only the distance between the Fermi level and the VBM on a pure CZTS surface and on a CZTS sample covered with CdS need to be measured to obtain the VBO.

Even though in principle the flat-band VB approach is equivalent to the direct VB and indirect VB approaches, the +0.41 eV spike-like CBO reported for the CZTS/CdS interface using this method [17] is by far the largest ever reported. Furthermore, the same type of measurement performed on different CZTS(e) samples with different S/(S+Se) ratios resulted in very similar CBO values, within 0.07 eV (Fig. 3). This contrast with nearly all other measurements and calculations, which show a substantial increase in the CBO when moving from a CZTS to a CZTSe absorber (Sec. 2, Fig. 3). In Sec. 6 and Sec. 8.1.2 we will propose two reasons why the CBO of the CZTS/CdS interface might be overestimated using the flat-band VB approach.

5.3. *Deviation in the reported band offsets*

We divide the possible causes of deviation into two categories. The first category is related to *real* variations in the CBO depending on the particular preparation conditions of CZTS(e) and CdS. The second category is related to errors in the *evaluation* of the CBO by experiment or computation. Those two categories will be examined in parallel in the next sections, which are divided by the mechanism that causes the variation.

Even though measurement errors may well exist, we already note at this point that they are unlikely to be the only reason for the wide range of measured CBOs. This becomes evident by plotting the measured CBO of each CZTS/CdS heterojunction as a function of the conversion efficiency of the resulting solar cell (Fig. 4). A rough correlation can be observed between the solar cell performance and the measurement of an optimal or nearly optimal CBO. In fact, all the solar cells with a cliff-like CBO between −0.34 eV and −0.18 eV (far from the optimal range) had efficiencies below 5%. Conversely, all solar cells with a CBO above −0.13 eV (within the optimal range or close to it) had efficiencies above 7%. Hence, it appears as if obtaining a spike-like CBO, or at least a nearly flat CBO, is both *possible* and *necessary* for high-efficiency devices.

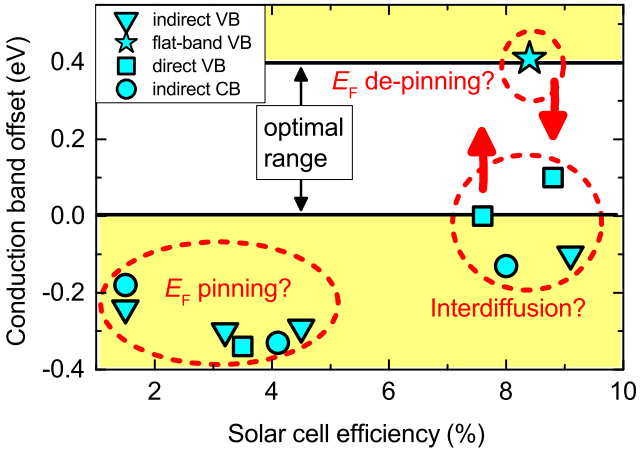

Figure 4: The measured CBOs at different CZTS/CdS interfaces versus the efficiency of the corresponding solar cells. In the cases where no solar cells were characterized in parallel with the band alignment measurement, we refer to devices reported in the same period of time by the same groups who fabricated the films used in the measurements [54–56]. In cases no efficiency reports could be found, the data point is not shown. A rough trend of increasing CBO with increasing efficiency can be established. It is proposed that: (i) the interfaces with the lowest CBO suffer from Fermi level pinning (Sec. 6); (ii) the high efficiency devices where a nearly flat CBO was measured might in reality have a higher CBO due to interdiffusion, which is not fully resolved in the measurement (Sec. 10), hence the upward arrow; (iii) the data point related to the flat-VB measurement might in reality have a lower CBO due to Fermi level de-pinning (Sec. 6), hence the downward arrow.

6. Role of Fermi level pinning

A first non-ideality that may cause deviation of the theoretical band alignment predicted by Eq. 1 is Fermi level pinning by crystal defects. The ideal situation of a CZTS/CdS interface without Fermi level pinning is illustrated in Fig. 5(a). There, the distance between the band edges and the Fermi level varies near the heterojunction due to electrostatic band bending. This corresponds to the potential drop caused by the negative (positive) charge present in CZTS (CdS) due to their ionized shallow acceptors (donors). The depth of the band bending region (depletion region) is more than 100 nm due to the moderate doping density of CZTS and CdS, set to 10^{16} cm^{-3} in all the simulated band diagrams of Fig. 5. As a completely different scenario, Fermi level pinning at the CZTS/CdS interface is illustrated in Fig. 5(c) and can be described as follows. If a very high density of charged defects ("pinning defects") exists either in the materials' bulk or at the interface, a large amount of charge will be present in the regions where those defects are ionized. For the case of bulk defects, such regions are delimited by the heterointerface on one side, and by the point where the Fermi level crosses the defect level on the other side. For certain combinations of pinning defect types and energies, for example a bulk acceptor in CZTS and a bulk donor in CdS as shown in Fig. 5(c), the defect levels must necessarily be ionized on both sides of the interface. In the example of Fig. 5(c) the pinning defect density is 10^{20} cm^{-3} for both the acceptor defect in CZTS and the donor defect in CdS. As the charge associated to ion-

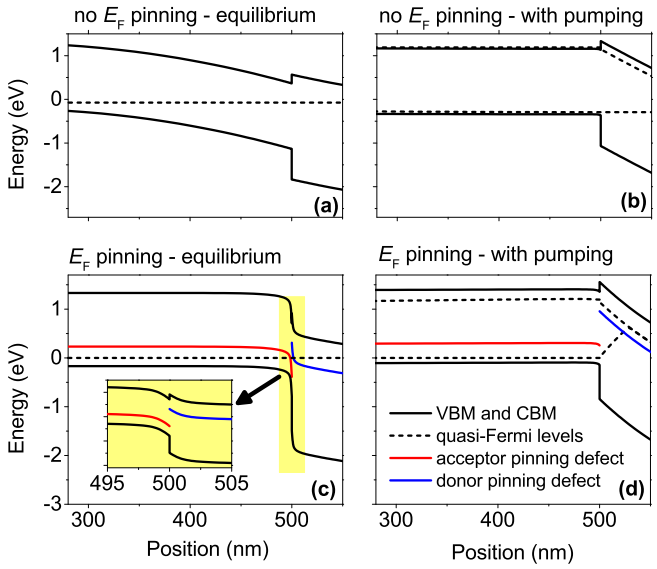

Figure 5: Simulated band diagrams of CZTS/CdS heterojunctions at zero applied voltage under different conditions, using the program SCAPS [57]. The doping density of both CZTS and CdS is kept constant at 10^{16} cm^{-3}. In (a) and (b) there are no charged defects in the bulk or at the interface (no Fermi level pinning). In (c) and (d) there is a bulk acceptor in CZTS 0.4 eV above the VBM and a bulk donor in CdS 0.6 eV below the CBM. Both defects have a density of 10^{20} cm^{-3}, and this pins the Fermi level at the interface. As evident from the inset of (c), the CBO is not modified strictly speaking. However, band bending occurs over such a narrow region that it is in practice equivalent to a CBO modification. The simulations in (a) and (c) are in the dark. The simulations in (b) and (d) are under monochromatic illumination at 800 nm with an intensity of 100 W/mm^2, which simulates optical pumping employed in [17] using the flat-band VB method. (b) demonstrates how band flattening is achieved in the flat-band VB approach. (d) demonstrates that, when Fermi level pinning exists in the dark, optical pumping can restore the ideal unpinned CBO ("Fermi level de-pinning"), leading to an error in the flat-band VB approach.

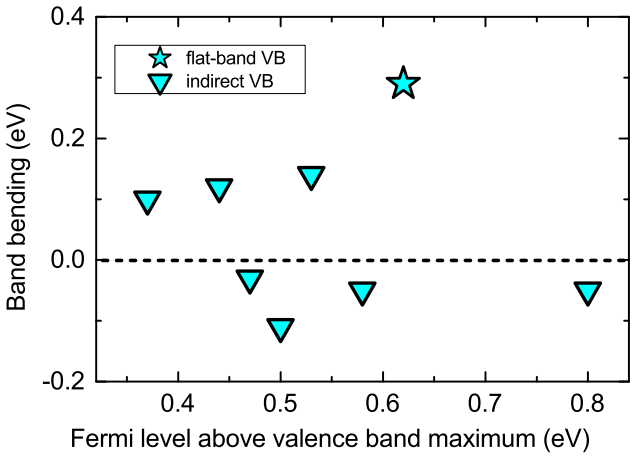

Figure 6: Measured band bending at different CZTS/CdS interfaces versus Fermi level position of CZTS above the valence band maximum (E_F – VBM) in bare CZTS. Data taken from different PES measurements [10, 13, 15, 17, 21–24]. Neglecting band bending in CdS, E_F – VBM + BB gives the Fermi level position at the interface with respect to the VBM of CZTS. No clear correlation can be identified, which indicates that the Fermi level at the interface is not pinned at the same energy in all samples. A positive (negative) band bending means that the bands bend downwards (upwards) from CZTS(e) to CdS. Note that in many cases the bands bend in the opposite direction to what is expected based on Fig. 5(a). Note also the particularly large bend bending measured with the flat-band VB approach.

ization of those defects is very large, steep band bending occurs over a very narrow region, which can be of the order of 1 nm (inset of Fig. 5(c)). Thus, one uses the expression "Fermi level pinning" to indicate that the Fermi level position within each material cannot exceed the energy position of the defect level, except for in a very narrow interface region. A similar situation can be obtained by replacing one of the two bulk defects with an interface defect of the same type (acceptor or donor) as the replaced defect.

Strictly speaking, the CBO remains the same as in the unpinned case, as evident from the inset of Fig. 5(c). However, since the interface band bending associated to Fermi level pinning is rather abrupt, it can be regarded in practice as an offset to the natural band alignment. In the example of Fig. 5(c), Fermi level pinning results in a CBO decrease by 1.0 eV with respect to the unpinned interface of Fig. 5(a). The opposite result (CBO increase) can be obtained, for example, by using a bulk pinning defect of donor type in CZTS and of acceptor type in CdS. The large simulated change in the band offsets by Fermi level pinning shown in Fig. 5(c) is not necessarily an exaggeration, as variations up to 1.2 eV in the band offsets have been reported before for other solar cell interfaces [58].

It is therefore mandatory to examine the possible dependence of the CBO of CZTS(e)/CdS solar cells on Fermi level pinning. In fact, considerable shifts in the expected band alignment have already been related to Fermi level pinning in other important solar cell interfaces, such as $CuInS_2$/CdS, CIGS/Zn(O,S), and Cu_2O/ZnO [37]. Some insights can be gained by plotting the measured band bending at different CZTS/CdS interfaces versus the distance (E_F – VBM) between the Fermi level and the VBM in a bare CZTS sample as determined by PES. This is shown in Fig. 6. If the interface Fermi level of all measured samples was pinned at a fixed energy with respect to the VBM of CZTS, band bending should decrease as (E_F – VBM) increases, as shown for example for the Cu_2O/ZnO interface [58]. However, according to the data in Fig. 6, this does not seem to be the case for the CZTS/CdS interface. Yet, the measured band bending is generally very small compared to what would be expected for an unpinned interface (Fig. 5(a)). In some cases, it is even of opposite sign than expected for a p-type absorber and an n-type buffer. This indicates that there is a limitation in the movement of the Fermi level within the band gap of CZTS, even though the Fermi level position at the heterointerface (equal to E_F – VBM + BB) varies from case to case. Therefore one may expect that the CBO is *decreased* by Fermi level pinning with respect to its natural value, as in the case simulated in Fig. 5(c) (a CBO *increase* would instead be accompanied by very large band bending).

The small band bending consistently observed at CZTS/CdS interfaces could be caused by (i) Fermi level pinning by a very high density of bulk/interface defects close to the Fermi level as in Fig. 5(c); (ii) Fermi level pinning by spontaneous forma-

tion of compensating defects near the interface as the Fermi level moves upward within the CZTS band gap [59]; or (iii) depletion of the bare CZTS surface, i.e., downward band bending occurring naturally at CZTS surfaces even without formation of an interface with an n-type material. Mechanism (iii) is unlikely because surface accumulation (rather than surface depletion) has been observed at CZTS(e) surfaces [25, 60, 61]. Mechanism (ii) is more plausible in CZTS than in CZTSe, as the "doping pinning rule" [59] predicts that (E_F − VBM) cannot exceed 1.15 eV in CTZS, whereas no limitation is expected for CZTSe [29]. Yet, the measured Fermi level position at the interface (equal to E_F − VBM + BB) is well below the 1.15 eV limit in all existing reports (Fig. 6) so no Fermi level pinning from spontaneous compensation is actually expected in theory. Mechanism (i) may well be the dominant one, but identification of the specific defects that pin the Fermi level is not straightforward. Possible candidates are: the Cu_{Zn} acceptor in the CZTS bulk; the V_{Cu} acceptor close to CZTS surfaces (which are more Cu-poor than the bulk in high-performance cells, thus accommodating a higher V_{Cu} density [60]); or surface acceptors due to, for example, unpassivated dangling bonds [33].

Since Fermi level pinning does not involve changes in the materials band gaps at the heterointerface but only a shift in the band offsets, the CBO under pinning conditions should in principle be measured correctly by all the approaches shown in Fig. 2 according to the discussion in Sec. 3. However, a peculiar error ("Fermi level de-pinning") may occur using the flat-band VB approach, as illustrated in Fig. 5(d). Since the CBO shift from Fermi level pinning is due to abrupt band bending from a narrow interface region with very high charge density, a large enough excess carrier population generated by the pump beam will screen the interface charge and re-establish the original (unpinned) band alignment (Fig. 5(d)). This phenomenon is conceptually identical to band flattening in the depletion region of an unpinned interface by the pump beam (Fig. 5(b)), which is the basic principle behind the flat-band VB measurement approach.

Therefore, the flat-band VB method may overestimate the CBO of a CZTS(e)/CdS interface where the Fermi level is pinned. An overestimated CBO should be accompanied by an overestimation of band bending by the same amount, due to the larger shift between pumped and unpumped PES spectra. Hence, a particularly large measured band bending could be a sign of an error in the CBO determination. Indeed, the band bending measured in [17] with the flat-band VB approach (0.29 eV for the CZTS/CdS interface) is by far the largest among all existing experimental reports, as evident from Fig. 6. Assuming that the real band bending is 0.0-0.1 eV, as in the majority of the other studies, this implies that the CBOs reported in [17] could be overestimated by about 0.2-0.3 eV. This is indicated by a downward arrow in Fig. 4.

7. Role of interface orientation

Orientation-dependent band alignment has been mentioned in earlier work as a potential cause of variability in the CBO of the CZTS(e)/CdS interface, without further investigation [63]. To the authors' knowledge, no studies exist on this subject. Regardless of the materials in question, orientation-dependent band alignment can occur when a nonzero orientation-specific dipole moment exists at the interface [64]. Specific conditions need to be met for this to occur. They are the following: (i) the surface of at least one of the two heterojunction materials must be polar [64]; (ii) the atomic layers on the two sides of interface plane must be heterovalent [40]; and (iii) any dipole-compensating interface reconstruction must not proceed to the point where the dipole moment is completely canceled [62]. Condition (i) is met, for example, at (001) surfaces of compound zincblende semiconductors [64]. In CZTS(e), the condition is met at the (001), (110), (112), and (100) surfaces due to the presence of alternating cationic and anionic layers along those directions. Condition (ii) is met in the classical example of a Ge/GaAs(001) interface from which the band alignment theory of polar interfaces was originally developed [62]. In the CZTS(e)/CdS system, the condition is met at the (001) and (110) interfaces as explained later in this section. Condition (iii) is in practice very difficult to check experimentally, even on monocrystalline interfaces. However, convincing experimental evidence of orientation-dependent band alignment has been shown for other zincblende semiconductor pairs from which the CZTS(e) kesterite structure is derived. Examples are Ge/GaAs(001) [65] and GaAs/ZnSe(001) [66]. The measured dipole contribution to the band alignment (up to a few hundred meV) was compatible with certain interface reconstruction patterns that did not cancel the dipole moment of the ideal unreconstructed interface completely [38].

It must be emphasized that the theory developed to model the influence of interface orientation on band alignment was intended for abrupt monocrystalline heterojunctions [62]. Thus, such a theory cannot be rigorously applied to the CZTS(e)/CdS system, which is a polycrystalline heterojunction with different grain orientations within the same sample and interdiffusion over regions of several tens of nm, which facilitates interface reconstruction. Also, transmission electron microscopy images of the CZTS(e)/CdS interface suggest that, even within a single CZTS(e) grain, the CZTS(e) surfaces at the heterojunction are not necessarily single-orientation, atomically smooth facets but that, instead, their orientation varies continuously [67, 68]. Nevertheless, based on qualitative arguments, here we suggest a reason to suspect that the band alignment of CZTS(e) solar cells is more likely to have some orientation dependence than the band alignment of CIGS solar cells.

The reason is that condition (ii) is not satisfied by any low-Miller index interface in the CIGS/CdS system, but it is satisfied by some low-Miller-index interfaces in the CZTS(e)/CdS system, namely the (001) and (110) interfaces. Differently from (100) and (112) surfaces, the (001) and (110) surfaces of CZTS(e) can be terminated by cationic planes that consist either of 50% Cu atoms and 50% Zn atoms (Fig. 7(a)) or of 50% Cu atoms and 50% Sn atoms (Fig. 7(b)). Such surfaces are heterovalent with their commensurate CdS surfaces, so they can generate an interface dipole that can shift the natural band alignment. The characteristics of the dipole can be predicted by solving with Poisson equation perpendicularly to the inter-

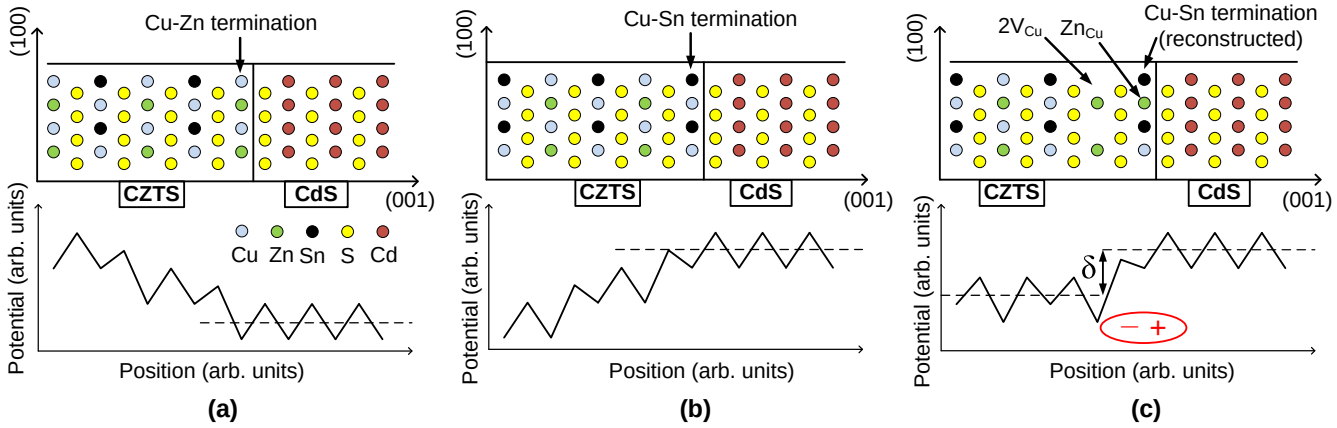

Figure 7: Potential across CZTS(001)/CdS(001) interfaces with different terminations, calculated by solving the Poisson equation perpendicularly to the interface using the approximations outlined in [62] ("theoretical alchemy"). The dielectric constants of CZTS and CdS are assumed to be equal for simplicity. (a): When CZTS is terminated by a Cu-Zn plane, the potential on the CZTS side diverges to an infinitely positive value. (b): When CZTS is terminated by a Cu-Sn plane, the potential on the CZTS side diverges to an infinitely negative value. (c): When CZTS is terminated by a Cu-Sn plane with a Zn_{Cu} defect every four atoms and two V_{Cu} defects every four atoms in the neighboring Cu-Zn plane, an interface dipole δ results without divergence of the potential.

face using the method outlined in [62] ("theoretical alchemy"). This is shown in Fig. 7. In the case of an unreconstructed Cu-Zn termination (Fig. 7(a)), the potential is predicted to increase and diverge on the CZTS(e) side, a phenomenon known as "electrostatic catastrophe" [62]. The same phenomenon, but with opposite sign of the potential, is predicted when an unreconstructed Cu-Sn plane is present at the interface (Fig. 7(b)). The two cases above are clearly not realistic and, in fact, first principles calculations show that the CZTS(e)/CdS(001) and CZTS/CdS(110) interfaces have a high interface energy [30] just like the classical Ge/GaAs(001) interface [64]. However, certain reconstruction patterns may stabilize the interface without completely canceling the interface dipole moment, as discussed theoretically in [62, 69] and demonstrated experimentally for Ge/GaAs(001) [65] and GaAs/ZnSe(001) [66].

In the case of the CZTS(e)/CdS interface, an example of how this could occur is shown in Fig. 7(c). A Cu-Sn terminated (001) surface is reconstructed by a Zn_{Cu} defect every four atoms in the Cu-Sn plane and by two V_{Cu} defects every four atoms in the adjacent Cu-Zn plane. This results in a potential shift δ at the interface (dipole layer) without a divergence of the potential in the CZTS bulk. Unfortunately, no calculations of the most likely reconstruction patterns stabilizing the (001) and (110) interfaces could be found, so the reconstruction pattern used in Fig. 7(c) is merely an example. Note that, even though the (100) and (112) surfaces of CZTS(e) are polar, they are not heterovalent with the commensurate (100) and (111) surfaces of CdS respectively, because their cationic planes consist of 50% Cu, 25% Zn, and 25% Sn. This means that, even though unreconstructed (112) and (100) *surfaces* are unstable due to the "electrostatic catastrophe" [70, 71], unreconstructed (112) and (100) *interfaces* are stable due to the image charge provided by CdS which stabilizes the potential. In fact, the CZTS(112)/CdS(111) interface was found to have the smallest interface energy among all the investigated interface orientations [30].

At a device level, the interface dipole δ causes a potential drop over a very narrow region across the interface (inset of Fig. 8(b)), which is in practice equivalent to an offset of the natural CBO by an amount equal to δ. From a device perspective, this effect is very similar to the effect of Fermi level pinning (Fig. 5(c)). For the case of the reconstructed Cu-Sn termination shown in Fig. 7(c), the CBO decreases by δ (Fig. 8(b)). For the opposite case of a reconstructed Cu-Zn termination (not shown), the CBO increases by an amount equal to the interface dipole of that case (Fig. 8(a)). This semi-quantitative argument is consistent with first-principle calculations on the unreconstructed CZTS(e)/CdS(001) interface [31], which found that the CBO changed depending on the CZTS(e) termination. For Cu-Zn-terminated CZTS, the CBO was less negative than for Cu-Sn-terminated CZTS [31]. This implies interface dipoles of the same sign as in our analysis.

Several authors have correctly remarked that orientation-dependent band alignment is not expected in the CIGS/CdS system [37, 38, 42]. That is due to the fact that (001)- and (110)-oriented interfaces are isovalent in the CIGS/CdS system because all cationic planes consist of 50% Cu atoms and 50% (Ga,In) atoms. Hence, those planes have the same overall valence as the Cd planes. As explained above, however, (001)- and (110)-oriented interfaces are heterovalent in the CZTS(e)/CdS system and therefore this is a significant difference between CZTS(e) and CIGS.

Nevertheless, we suggest that orientation-dependent band alignment is unlikely to be a major reason behind the deviation of the measured CBOs in CZTS(e)/CdS solar cells. That is because the preferential CZTS(e) orientation in the substrate normal direction does not differ much among thin films grown by different workers and the preferential orientation is actually very similar for CIGS, CZTSe, and CZTS [72]. The above statement can be checked by comparing the relative intensity of different x-ray diffraction (XRD) peaks in different films when the XRD measurement is performed with a symmetrical (Bragg-Brentano) geometry. Also, exposed CZTS(e) facets

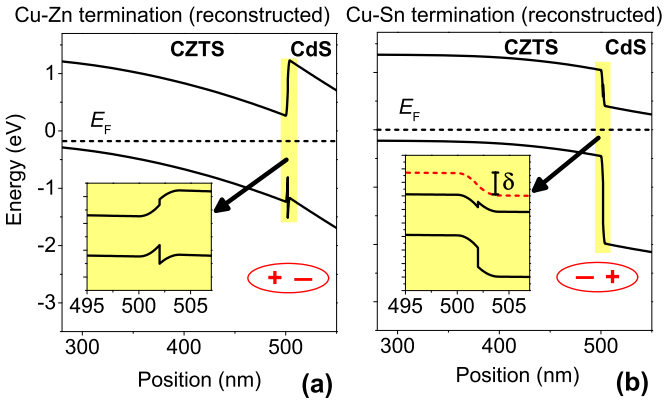

Figure 8: Simulated band diagrams of CZTS/CdS heterojunctions in the dark at zero applied voltage, using the program SCAPS [57]. (a): A CZTS(001)/CdS(001) interface terminated by reconstructed Cu-Zn planes is simulated by two charge layers of 2 nm depth and $\pm 10^{20} q$ cm^{-3} charge density, where q is the elementary charge. The positive charge layer is on the CZTS side and the negative charge layer is on the CdS side. Even though the original CBO is maintained strictly speaking (inset of (a)), band bending caused by the interface dipole δ occurs over such a narrow region that it can be considered as an increase in CBO in practice. Note that the sign of the potential drop at the interface is compatible with Fig. 7(c) but it appears to be of opposite sign because the *electron* energy is plotted in the band diagrams, which is of opposite sign as the potential. (b): A CZTS(001)/CdS(001) interface terminated by reconstructed Cu-Sn planes is simulated by switching the sign of the charge layers in (a). The CBO is decreased with respect to the dipole-free case.

usually do not appear atomically smooth but their orientation varies continuously within the same grain, as mentioned before. A more likely effect, illustrated in Fig. 9(a), is lateral (in-plane) band alignment variations from grain to grain. Unfortunately, the properties of single grains cannot be resolved in a photoemission experiment because CTZS(e) grains are micron-sized at best and the lateral resolution of PES is not better than tens of μm. Then, grain-to-grain band alignment variations would result in broadening of the core level peaks and tailing of the valence band spectrum when a CZTS(e) sample with a thin CdS overlayer is measured (PES-3 measurement in Figs. 2(a), 2(c)). Since orientation-dependent interface dipoles do not influence the materials band gaps, the additional dipole component δ is correctly included in the CBO measured by all the approaches shown in Fig. 2 according to the discussion in Sec. 3.

If preferential orientation of the exposed CZTS(e) surfaces could be controlled to produce (001) or (110) polar facets that are heterovalent with the buffer layer, the CBO of CZTS(e)/CdS interfaces could in principle be engineered by the interface dipole layer. This could be achieved, for example, by development of an orientation-dependent etchant, similarly to potassium hydroxide etching of Si, which is routinely used to produce (111) Si surfaces.

8. Role of band gap changes

8.1. CZTS(e) band gap

8.1.1. Cation disorder

CZTS(e) thin films always feature some cation disorder in the Cu/Zn sublattice, due to the low formation energy of the (Zn_{Cu}+Cu_{Zn}) defect pair. The degree of disorder can be quantified by the order parameter of the material [73, 74]. The band gap of CZTS(e) was shown to decrease by 0.20 eV in CZTS [75] and by 0.11 eV in CZTSe [74] when the order parameter of the materials decreased from a realistically achievable high-order state to a fully disordered state. The effect of those changes on the interface CBO can be predicted by estimating the direction of the corresponding band edge shifts with respect to a reference level. According to first principles calculations [76] the band gap decrease should occur more through an upward shift of the VBM than through a downward shift of the CBM. Therefore, the CBO should only be marginally affected by the order parameter. Since cation disorder affects the *bulk* band gap of the material, it does not cause an error in the measurement of the CBO, provided that the modified bulk band gap is correctly measured.

8.1.2. Tail states

Another issue is the definition of band gap in CZTS(e) [77]. Tail states are frequently observed within the band gap of the extended states due to band gap- or electrostatic potential fluctuations caused by secondary phase inclusions or acceptor-donor defect clusters. Those fluctuations can occur both in the out-of-plane (transport) direction, and in the in-plane directions, which are defined in Fig. 9. In top-performing CZTS (CZTSe), the band gap including tail states is roughly 0.15 eV lower (0.02 eV lower) than the band gap of the extended states [54, 78]. The main possible consequence of CZTS(e) tail states on the band alignment is lateral variations in the CBO and VBO. In the case of band gap fluctuations, the CBO increases from regions of higher band gap to regions of lower band gap. Conversely, in the case of electrostatic potential fluctuations the CBO should remain constant (Fig. 9(b)) unless the potential fluctuations result in local interface dipoles.

If the CBO is defined as the offset between the edges of the extended states, then the CBO measured on materials with band tails should be equal to the CBO measured on tail-free materials, as long as the tails can be discerned from the extended states in the measurement. This means that the leading edge of the PES or IPES signal must be correctly extrapolated to the onset of the extended states. The tail states must be recognized as a tail in the photoemission signal and disregarded in the extrapolation procedure. However, for materials with a high density of tail states like CZTS and CdS, this can be a difficult task which may increase the measurement uncertainty.

An interesting example is related to the particularly large CBO reported in [17] for the CZTS/CdS interface. It was pointed out earlier in this paper (Sec. 6) that the CBO in that study could have been overestimated due to the possibility of Fermi level de-pinning in the flat-band VB measurement approach. An additional reason for CBO overestimation could just be the uncertainty in the extrapolation of the PES signal. In fact, inspection of Fig. 2(c) in Ref. [17] reveals that extrapolation of the PES leading edge in that sample is not a trivial task (**EX** label in Fig. 3). In our opinion, a fit to a 0.3 eV lower binding energy than the one determined by the authors could be just as realistic. This would imply a CBO of about +0.1 eV as opposed to

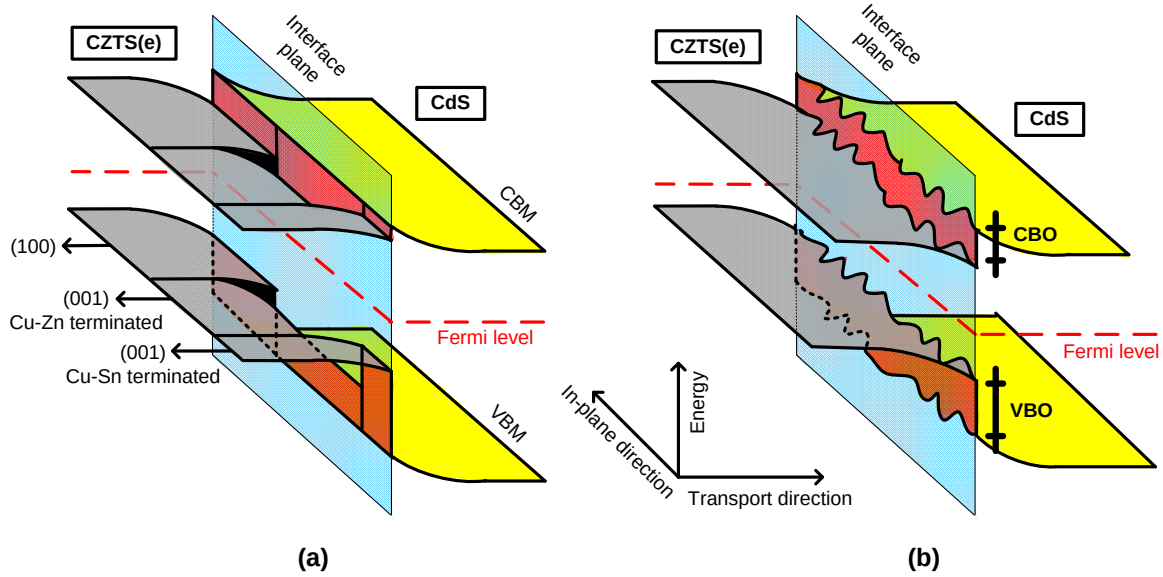

Figure 9: Band diagrams of CZTS/CdS heterojunctions along two directions: the transport direction (out-of-plane) and a direction contained in the interface plane. (a): CBO variations in the interface plane due to differently oriented crystal grains. The (100)-oriented grain does not have a dipole component in the CBO. Conversely, the (001)-oriented grains have a dipole component (Fig. 8), which modifies their natural CBO. (b): Electrostatic fluctuations in CZTS in the interface plane, which result in fluctuating band edges without modification of the band alignment, unless the fluctuations generate interface dipoles.

the reported value of +0.41 eV. Interestingly, fitting the leading edge of the spectra from the CdS/CZTSe and CdS/CZTSSe interfaces in the same study appears to be more straightforward.

8.2. CdS band gap

8.2.1. Mix of phases

In the case of CdS, a number of physical mechanisms have been shown to alter its band gap. First of all, there exist two CdS phases, cubic (zincblende) and hexagonal (wurtzite), with very similar formation energies. The wurtzite phase has a band gap that is about 0.1 eV larger than the zincblende phase (roughly 2.5 eV versus 2.4 eV). Those two phases are often found to coexist in CdS made by chemical bath deposition [79], which is the standard technique used to deposit CdS in CZTS(e) solar cells. According to first-principles calculations [30, 80], the band shift seems to occur primarily in the conduction band, which is expected to lie 0.1 eV higher in wurtzite CdS. This corresponds to the data point labeled as **W** in Fig. 3 for the only calculation performed with wurtzite CdS. The likely coexistence of zincblende and wurtzite CdS phases is similar to the case of band gap fluctuations in CZTS(e) discussed in the previous section. It is expected to generate lateral CBO variations rather than an overall CBO shift. If the CdS layer is a mix of the two phases, its bulk band gap is not clearly defined. The measured band gap value will depend on the relative amount of the two phases. Therefore, the measured CBO will vary depending on the measured bulk band gap but the error will be small since the band gap difference between the two phases is only 0.1 eV.

8.2.2. Quantum confinement

The band gap of CdS expands due to quantum confinement effects if the crystallite size is small enough to be comparable to the Bohr radius of the material (about 3 nm [81]). This can potentially be a crucial effect: band gap changes due to quantum confinement in (Zn,Sn)O films grown by atomic layer deposition are so large that they have been successfully controlled to engineer the desired CBO in Cu(In,Ga)Se_2/(Zn,Sn)O heterojunction solar cells [82]. It has been shown that the band gap of CdS starts to increase at a particle size of 6 nm and reaches roughly 3.5 eV for a crystallite size of 1 nm [83]. We note that CdS films by chemical bath deposition are always nanocrystalline and that the "seed layer" that first forms on the CZTS(e) surface typically has a smaller crystallite size than the final film [79, 84]. Because the band gap that determines the band alignment with CZTS(e) is that of the seed layer, the interface band gap is possibly higher than that measured in the film with the desired thickness by optical measurements. In fact, in [85] the band gap of CdS increased by 0.15 eV as film thickness decreased from 200 nm to 35 nm, possibly due to quantum confinement effects from the smaller crystallite size in the thinner films. Unfortunately, no studies on the corresponding band edge shifts are known to the authors. By assuming variations up to 0.2 eV in the band gap of the CdS seed layer depending on preparation conditions, and by assuming that band gap expansion occurs through an upward shift of the conduction band as demostrated, for example, in (non-hydrogenated) amorphous Si [86] and amorphous (Zn,Sn)O [82] one may expect a ±0.1 eV deviation in the CBO. If quantum confinement occurs over the whole CdS film thickness, like in (Zn,Sn)O [82], it does not result in a CBO measurement error as long as the modified bulk band gap is correctly measured. However, if quantum confinement is limited to the seed layer near the interface, the band gap change is more difficult to measure and will result in a CBO measurement error if the effect is not detected.

8.2.3. Epitaxial growth

A third mechanism that may modify the interface band gap of CdS is strain in the CdS lattice induced by formation of the interface with CZTS(e). This mechanism depends strongly on the growth mode of CdS, especially on whether CdS grows epitaxially on CZTS(e). Up front, one may expect a larger modification for CZTS/CdS interfaces than for CZTSe/CdS interfaces due to the larger lattice mismatch of the former (7% versus 2.6% respectively).

As discussed in Sec. 2, an epitaxial interface is always employed in first-principle calculations as it allows one to use much smaller periodic structures, thus reducing computational time. However, some studies [28, 29] subtracted the effect of interface strain on the band structure of CdS and modeled therefore the "natural" band alignment of a non-epitaxial interface where both materials are at their equilibrium lattice constant. They are labeled **N** in Fig. 3. Other studies, which we will discuss briefly in the following, modeled a strained epitaxial interface by including strain-induced band gap variations in CdS [27, 30, 33]. They are labeled **EP** in Fig. 3. In [30] the band gap of CdS at the strained CZTS/CdS interface was extracted from separate CdS bulk calculations, where the CdS lattice constant in the plane of the interface was fixed to a value equal to the CZTS lattice constant and the CdS lattice constant in the direction perpendicular to the interface was free to vary. With this approach, the CdS interface band gap decreased by a significant amount (0.2-0.5 eV) depending on the interface orientation. In [33] the CdS band gap was free to vary in the CZTS/CdS interface calculation itself, while the lattice constant in the interface plane was constrained to the lattice constant of CZTS and the lattice constant in the perpendicular direction was free to vary. Differently from [30], the interface band gap of CdS decreased by a negligible amount in this study. However, both studies calculated a CBO that was roughly 0.3 eV larger than the "natural" CBO (Table 2).

Therefore, there are some indications that epitaxial growth of pure CdS on pure CZTS(e) may increase the CBO significantly. Interestingly, epitaxial CZTS(100)/CdS(100) and CZTS(112)/CdS(111) interfaces have been demonstrated by some authors in actual solar cells [68, 87]. However, CZTS and CdS have a relatively large lattice mismatch (7%), which makes epitaxial growth unlikely. Then, we suppose that an epitaxial interface is made possible by Cd diffusion into CZTS and Zn diffusion into CdS, which are both often observed experimentally and are treated in detail in Sec. 10. Cd inclusions increase the lattice constant of CZTS [88], whereas Zn inclusions decrease the lattice constant of CdS [45], thus enabling a better lattice match at the interface. For this reason, it is likely that real epitaxial CZTS/CdS interfaces have much lower strain than 7% due to interdiffusion. Hence, the influence of epitaxial growth on the CBO is probably small. A similar argument applies to the CZTSe/CdS interface. Note, finally, that in polycrystalline materials epitaxial growth may only occur at certain locations due to the different grain orientations. In such a scenario, lateral variations of the CBO would exist.

9. Role of surface modifications in CZTS(e)

9.1. Etching

Modifications in the band edge positions at the CZTS(e) surface compared to the CZTS(e) bulk can be the result of growth conditions, annealing or etching. In CIGS absorbers, it is widely accepted that a Cu-poor surface causes the surface VBM to shift downwards and the band gap to expand [89]. A Cu-poor surface in CIGS can be achieved either by tuning the growth conditions or by performing a potassium cyanide (KCN) etching step before CdS deposition. It was similarly shown that a KCN etching treatment on CZTS increased its surface band gap from 1.5 eV to 1.9 eV through a downward shift of the VBM [10]. Hence the VBO with CdS became smaller but the CBO remained nearly unaffected, see **ET** in Table 1 and Fig. 3. Nevertheless, it cannot be excluded that other types of etching treatments [90] affect the CBO by a significant amount, even though the band alignment of CZTS(e) etched with alternative etching agents has not yet been measured. Since etching modifies the *surface* band gap of CZTS(e), its influence on the CBO can be captured by the direct/indirect CB approaches but not by the direct/indirect/flat-band VB approaches, according to the discussion in Sec. 3.

9.2. ZnS(e) segregation

Another possible surface modification is related to secondary phase segregation at the CZTS(e) surface. The most likely secondary phase is ZnS(e), due to the Cu-poor Zn-rich growth conditions required to achieve efficient solar cells [4, 91, 92]. A maximum in Zn concentration at the heterointerface is sometimes found [87, 93, 94] indicating segregation of Zn-rich phases. In some cases, ZnS(e) is intentionally etched with HCl [92]. There are two qualitatively different mechanisms of ZnS(e) segregation: the first is formation of a thin continuous layer, the second is formation of isolated ZnS(e) phases at a surface that mostly consists of CZTS(e). We argue that the latter is more likely for three reasons. The first is that isolated segregation has been observed directly by microscopy [91, 92]. The second is that a continuous thin ZnS(e) layer at the CZTS surface should be detected indirectly by the absence of a Cu and Sn signal using highly surface-sensitive composition-probing techniques such as x-ray photoemission spectroscopy (XPS) or secondary ion mass spectroscopy (SIMS). However, studies performed with such techniques consistently reveal a significant amount of Cu and Sn in Zn-rich CZTS(e) films [4, 95]. The third reason is that a ZnS(e) surface layer should be easily detected when measuring the VBM of a bulk CZTS sample with respect to the Fermi level, as routinely done in most band alignment studies shown in Fig. 3. This is because ZnS(e) has a much higher band gap than CZTS(e) and is n-type instead of p-type, hence its VBM should be much more distant from the Fermi level than in CZTS(e), in the case of a continuous ZnS(e) surface layer. Assuming that the above argument is correct, the measured CBO is expected to be the CBO of the actual CZTS(e)/CdS interface. However, since the CZTS(e)/ZnS(e) interface features a very large spike [30, 91], the actual behavior of the solar cell will depend on the geometrical details of the

ZnS(e) phases. The main expected consequence of scattered ZnS(e) phases at the heterointerface is an increase in series resistance with respect to the ZnS(e)-free case, as often discussed in the literature [4, 96, 97]. One may also expect a modification in the band alignment by oxide phases at the CZTS(e) surface. However, it has been shown that the alkaline NH_4OH-based chemical bath used by most researchers to deposit the CdS buffer layer removes almost completely the surface oxide grown by air exposure or air annealing [25].

9.3. Surface band gap narrowing

An intrinsic modification of CZTS surfaces (but not of CZTSe surfaces) was recently proposed on the basis of first-principle calculations [33]. It consists of an upward shift (by roughly 0.2 eV) of the VBM of bare CZTS surfaces, which is maintained even after interface formation with CdS. No changes in the CBM were predicted in [33], so the only influence on the band alignment would be an increase of the VBO by 0.2 eV. Experimental studies are needed to determine whether the modified VBM position predicted by theory is detected as a VBM shift or as a valence band tail in a PES measurement. In the former case, the CBO would be measured correctly by CB-based approaches due to the equivalence of surface and interface band gaps of CZTS, but it would be underestimated by VB-based approaches. In the case of a valence band tail, no errors in the CBO determination are expected.

9.4. Surface accumulation

Finally, both CZTS and CZTSe bare surfaces have been found to be in accumulation up to 0.15 eV [25, 60, 61] rather than in depletion as CIGS surface [61]. The reason for this is not completely clear. It seems to be related to a higher abundance of acceptor defects like V_{Cu} at the Cu-depleted surfaces [60], even though the intrinsic surface modification discussed above might also play a role [33]. Surface accumulation does not affect the direct VB and direct CB measurement approaches, as no measurements are performed on bare surfaces. Even using the other approaches, surface accumulation should result in neither a VBO nor a CBO measurement error. In fact, even though the VBM position in the PES-1 measurement in Fig. 2(a) is closer to the Fermi level than in the bulk due to accumulation, the larger shift of the CZTS(e) core levels between the PES-1 and PES-3 measurements compensates this effect exactly. The only consequences are underestimation of (E_F − VBM) and overestimation of band bending. The surface band bending due to surface accumulation can actually be determined by the flat-band VB method by comparing an unpumped and a pumped spectrum on a bare CZTS(e) surface [60].

10. Role of interdiffusion

Chemical interdiffusion across the heterointerface has already been shown to be a major force in determining the band alignment of many other heterojunction solar cells, often beneficially. In Cu_2O/ZnO solar cells, significant CBO variation (up to 0.4 eV) was observed depending on the presence or absence of a CuO interface phase induced by the particular process conditions chosen for deposition of the ZnO heterojunction partner [98]. In CIGS/CdS solar cells, Cd and S can diffuse into CIGS, and In and Se can diffuse into CdS [99, 100]. Especially Se inclusion into CdS was shown to decrease its band gap (from 2.4 eV to 2.2 eV) 20 nm away from the interface [101]. The same effect was observed in CZTSe/CdS solar cells [12]. In CdTe/CdS solar cells, S and Te can interdiffuse to a depth over 200 nm and form a $CdTe_{1-x}S_x$ interface phase with an intermediate band gap [102].

10.1. Cd

In CZTS(e) solar cells, diffusion of Cd into the absorber is ubiquitously observed as a tail in the Cd signal into the CZTS(e) layer in elemental depth profiling experiments [19, 54, 93, 103]. Tails between 10 nm long [2, 87, 94] and 50 nm long [54, 93] have been reported. The most likely mechanism of Cd incorporation into CZTS(e) is by Zn substitution, Cd_{Zn} [88, 104]. The effect of this chemical modification on the properties of CZTS was studied in [88]. It was found that the CZTS band gap decreased by 0.2 eV and its lattice constant increased from 5.44 Å to 5.50 Å as the Cd/(Cd+Zn) ratio increased from 0 to 0.5. The corresponding band edge shifts can be guessed based on qualitative arguments. Referring back to Sec. 5, the VBM and CBM of CZTS(e) are based on antibonding states. Increasing the lattice parameter by Cd substitution decreases the repulsion between bonding and antibonding states, therefore both the VBM and CBM are expected to shift downward. As the experimental band gap decreases by Cd substitution, it is concluded that the CBM shift is larger than the VBM shift. We note that the band alignment between Cu_2CdSnS_4 and Cu_2ZnSnS_4 was studied in [105] by first-principles calculations. Even though the states responsible for the VBM were found to shift downwards in Cu_2CdSnS_4 as expected from the above arguments, the calculation predicted that the VBM of the two materials should lie at the same energy. This unexpected result was obtained because an antibonding state from Cd *d* - S *p* orbital hybridization turned out to be at a slightly higher energy than the antibonding state from Cu *d* - S *p* orbital hybridization that is responsible for the VBM in Cu_2ZnSnS_4. Nevertheless, in our interface model we still assume a slight VBM downshift upon interdiffusion for three reasons. First, the distance in energy between Cu-, Zn-, and Cd *d* states is very small [105] so a more detailed study is needed to confirm that Cd *d* states actually become responsible for the VBM of Cu_2CdSnS_4. Second, the calculated density of states of Cd *d* orbitals near the VBM is much lower than the calculated density of states of Cu *d* orbitals near the VBM [105] so it is unclear whether Cd *d* states actually contribute to the VBM. Third, the density of Cd *d* states at the CZTS(e)/CdS interface with interdiffusion is lower than in the bulk Cu_2CdSnS_4 calculation because Cd replaces Zn only partially. Assuming Cd/(Cd+Zn) = 0.5 at the CZTS/CdS interface, our model implies that the CBM of CZTS is down-shifted by more than 0.2 eV. Such a situation is sketched Fig. 10. A qualitatively similar effect is expected for CZTSe, as shown in Fig. 11.

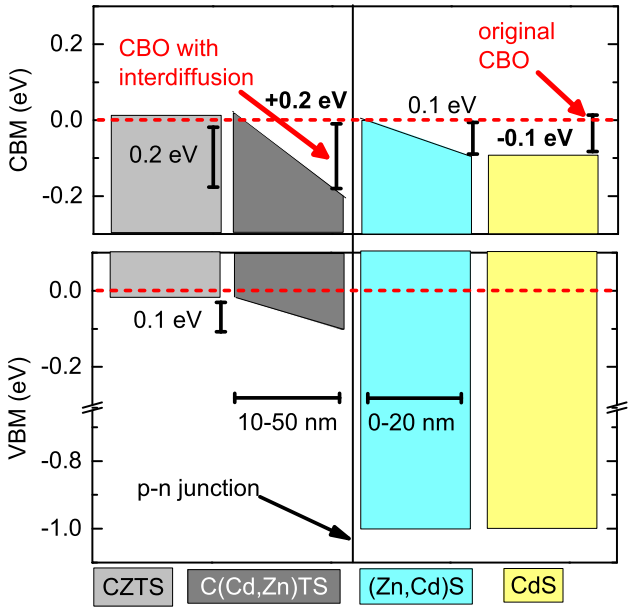

Figure 10: Semi-quantitative model of a (favorable) band alignment at the CZTS/CdS interface achievable in the presence of significant interdiffusion and assuming an unfavorable cliff-like CBO of -0.1 eV at the original CZTS/CdS interface without interdiffusion. The only band edge shifts considered are due to formation of C(Cd,Zn)TS and (Zn,Cd)S solid solutions at the interface. Electrostatic band bending is ignored.

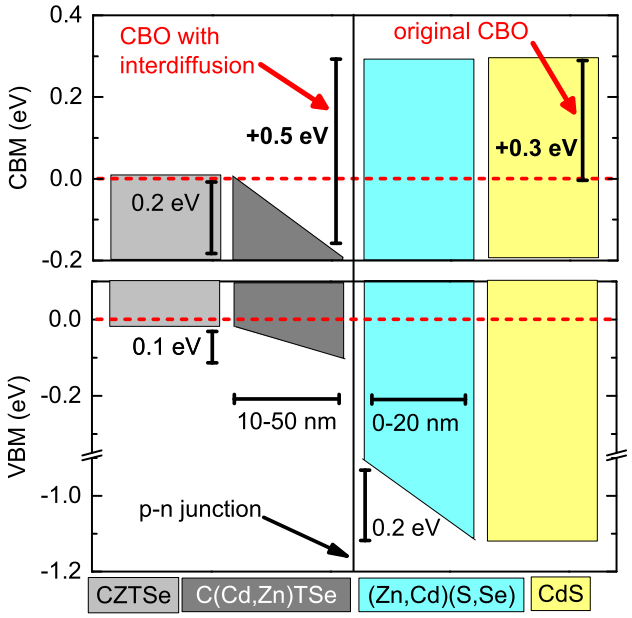

Figure 11: Semi-quantitative model of an (unfavorable) band alignment at the CZTSe/CdS interface achievable in the presence of significant interdiffusion and assuming an favorable spike-like CBO of +0.3 eV at the original CZTSe/CdS interface without interdiffusion. The main difference with the CZTS/CdS interface is the additional Se diffusion into CdS.

10.2. Zn

The CdS side of the junction is also affected by interdiffusion. Zn is often observed to diffuse from CZTS(e) into CdS [2, 19, 54, 87, 93, 94], which probably results in formation of a $Zn_{1-x}Cd_xS$ solid solution. Since ZnS has a smaller lattice constant and a larger band gap than CdS, the expected consequences of Zn interdiffusion are a lattice constant decrease and a band gap increase in CdS. According to the common anion rule and to experimental and computational reviews [37, 45, 48] the band gap increase should occur predominantly through a CBM up-shift, as sketched in Fig. 10. Interestingly, the decrease in the lattice constant of CdS due to Zn incorporation, combined with the increase in the lattice constant of CZTS due to Cd incorporation reduces the lattice mismatch between the two materials. For example, assuming interface compositions of Cd/(Cd+Zn) = 0.5 on the CZTS side and Zn/(Zn+Cd) = 0.75 on the CdS side, the lattice mismatch is reduced from 7% to under 0.5%. This might be the reason why epitaxial CZTS/CdS interfaces can be achieved under significant interdiffusion [68, 87], but they may be difficult to achieve using pure materials.

10.3. Se

In Se-containing absorbers, Se diffusion from CTZS(e) to CdS may also modify the band alignment. Se interdiffusion has been observed both in CZTSe/CdS solar cells [2, 12, 19] and in CIGS/CdS solar cells [101]. With both types of absorbers, it was possible to detect a 0.2 eV decrease in the band gap of CdS 10-20 nm away from the heterointerface using a combination of IPES and PES [12, 101]. This is compatible with the fact that CdSe has a smaller band gap than CdS. According to band alignment reviews [37, 45], the band gap change should occur both by a VBM up-shift and by a CBM down-shift. However, based on our earlier discussion we hypothesize that concurrent Zn interdiffusion may roughly compensate the CBM down-shift. Therefore, the resulting $Zn_{1-x}Cd_xS_ySe_{1-y}$ solid solution obtained in [12] may have the same CBM as CdS but a higher-lying VBM, as illustrated in Fig. 11.

10.4. Consequences

Even though the band alignment modification proposed in Figs. 10 and 11 is only based on semi-quantitative arguments, it does give a rough picture of what is likely to happen in real solar cells. In fact, it is compatible with the only depth-resolved band alignment measurement known to the authors [19], performed with the direct VB approach. In that study, the VBM of CZTS(e) shifted downwards by 0.1-0.2 eV close to the interface, corresponding to the region of Cd diffusion into CZTS(e) as modeled in Figs. 10 and 11. In the same study, the VBM of CdS shifted upwards when a pure selenide CZTSe absorber was used, as modeled in Fig. 11. The magnitude of the shift was found to be correlated to the amount of Se and Zn that diffused into CdS. However, the upward VBM shift of CdS was negligible when using a pure sulfide CZTS absorber, which is also compatible with our model in Fig. 10.

Unfortunately, the effect of interdiffusion on the CBO is difficult to capture by most experimental approaches shown in Fig. 2. The indirect VB approach and the flat-band VB ap-

proach can in principle measure the correct VBO by detecting the VBM shift due to interdiffusion in their interface measurement (PES-3 and FB-PES-3 in Fig.2(a) and Fig.2(e) respectively). However, they will underestimate (overestimate) the CBO if the difference between the CdS and CZTS(e) band gaps increases (decreases) at the interface with respect to its bulk value, as explained in Sec. 3. Assuming the interface modifications shown in Figs. 10 and 11, the indirect VB and flat-band VB approaches will underestimate the CBO of the CZTS/CdS interface by 0.2 eV and overestimate the CBO of the CZTSe/CdS interface by 0.1 eV. This is an important conclusion, since it implies that the real CBO at the CZTS/CdS interface may be systematically larger than the reported values in Table 1, provided that appreciable interdiffusion takes place. This is schematically shown by the upward arrow in Fig. 4.

The depth-resolved direct VB approach, as implemented in [19], can in principle distinguish the VBM shifts due to interdiffusion from those due to electrostatic band bending, since they occur over different length scales. Combined with compositional profiling, the amount of interdiffusion and the corresponding CBM shifts at the interface can then be guessed roughly. The indirect CB approach can (at least partially) capture the interface band gap change in CdS due to interdiffusion, as long as the IPES-2 measurements in Fig. 2(b) is performed close enough to the heterointerface, so that the *surface* band gap of CdS is a reasonable approximation of its *interface* band gap, according to the discussion in Sec. 3. In [12], this method revealed a narrowed CdS band gap 12 nm away from the interface. However, it is not possible to capture similar band gap changes in CZTS(e) because those changes occur *after* the interface has been formed. Therefore, the near-interface region of CZTS(e) must be analyzed after growing CdS to detect the effects of interdiffusion, which leaves the (depth-resolved) direct CB approach as the only possibility among the measurement schemes presented in Fig. 2. This approach has not been employed in any of the studies presented in Table 1. Unfortunately, ion beam etching can affect the conduction band features of CZTS(e) (see Sec. 11) and the IPES equipment necessary to implement the direct CB approach is not as readily available as UPS or XPS equipment. An alternative strategy could be to utilize a modified version of the direct VB approach, where the (bulk-sensitive) gap-1 and gap-2 measurements in Fig. 2(c) are performed by a non-destructive method which allows the outcome of the measurement to be fitted to a parametric model of the depth dependence of the band gap. A candidate technique is spectroscopic ellipsometry, which can accurately extract the optical functions of thin film stacks as long as certain conditions are met [106].

11. Role of measurement artifacts

A problem related to the depth-resolved direct VB (and direct CB) approaches is that depth resolution is achieved through ion beam etching of the sample. It is well known that prolonged energetic ion beam etching can lead to surface modifications due to preferential sputtering of the constituent elements of the material [37]. This was found to alter the band edge positions in CIGS [101]. In CZTS(e), it was observed that valence band features are preserved for Ar^+ ion beam energies as high as 1 kV [15]. However, it was reported elsewhere that a lower Ar^+ ion beam energy (400 eV) was already high enough to alter certain conduction band features [12]. In [10], an ion beam energy of 100 eV was recommended for etching CZTS(e) when employing the indirect CB measurement approach, even though the purpose of etching in that study was simply to remove the native oxide. One may conclude that the depth-resolved direct VB approach is easier to implement in practice than the depth-resolved direct CB approach, since valence band features appear to be more robust than conduction band features when CZTS(e) is subject to ion bombardment. A way to avoid ion bombardment in depth-resolved measurements could be to grow CdS on CZTS(e) *in situ*, and record PES or IPES spectra during growth, as done in [12] (related data points are labeled **G** in Fig. 3). However, there are problems with this approach: (i) CdS has to be grown with a vacuum-based technique, unlike the much more commonly used chemical bath deposition; (ii) the effects of interdiffusion on the CZTS(e) band edges cannot be captured, as CZTS(e) spectra are measured before CdS is grown; and (iii) the structure of CdS may not be fully developed in the initial stages of deposition, so it may be necessary to rely on indirect approaches, which are not depth-resolved.

Another potential measurement artifact is related to the presence of a native oxide layer on the surfaces to be analyzed, unless the materials are grown *in situ*. However, based on the above discussion, a short low-energy ion beam etching step seems to be sufficient to remove the native oxide without altering the band structure of the original materials. An alternative procedure, involving a short in-situ annealing before measurement, is outlined in [60].

12. CZTS(e)/CdS band alignment engineering by interdiffusion

Having ascertained that there can be many possible sources of variation in the CBO of CZTS(e)/CdS heterojunctions, we conclude that the CBO is not a fixed property of those material pairs. In the case of CZTS, the risk is to obtain a too low CBO (cliff-like). In CZTSe, the risk is to obtain a too high CBO (spike-like). Both such non-ideal cases have been documented in the literature, as shown in Fig. 3. While most of the CBO-varying mechanisms presented in the previous sections are not easily controllable by the experimentalist, here we propose how control of interdiffusion at the heterointerface can be used to engineer the desired band alignment. As suggested in [3], the temperature of a CdS post-deposition annealing step may be the most effective way to control the amount of interdiffusion. The CdS deposition temperature may also play a role, even though no specific studies are available in the literature to confirm it.

12.1. The case of CZTS

From the measured and calculated CBOs of the CZTS/CdS interface (Fig. 3), it seems as if this interface can easily have a detrimental cliff-like CBO. However, interdiffusion between

	Real increase (↑) or decrease (↓)		Overestimation (O) or underestimation (U) of CBO by different measurement approaches				
Mechanism	CBO	VBO	indirect VB	indirect CB	direct VB	direct CB	flat-band VB
1)Fermi level pinning	↓	↑	none	none	none	none	O
2)Polar interface	↕ L	↕ L	none	none	none	none	none
3)CZTS(e) disorder	↑ (small)	↑	none	none	none	none	none
4)Wurtzite CdS	↑ L	none	none	none	none	none	none
5)Quantum confinement	↑	none	U	U	U	none	U
6)Epitaxy	none	↓ L	O	O	O	none	O
7)Etching (KCN)	none	↓	O	none	O	none	O
8)Interdiffusion	↑	↓	U(O)*	U(O)*	U(O)*	none	U(O)*

Table 3: Estimated consequences of various physical and chemical mechanisms on the CBO and VBO at the CZTS(e)/CdS interface, based on the discussion in the main text. ↕: both an increase and a decrease in the CBO are possible. L: lateral (in-plane) inhomogeneity in the CBO is expected, rather than an overall modification of the CBO. U(O)*: underestimation of the CBO at CZTS/CdS interfaces and overestimation of the CBO at CZTSe/CdS interfaces.

CZTS and CdS may improve the situation by increasing the CBO up to a positive spike. The more Cd diffusion into CZTS, the more Cd_{Zn} substitution. This has two beneficial effects: (i) downward shift of the CBM, which increases the CBO, and (ii) downward shift of the VBM, which decreases the hole population, a key factor in reducing the interface recombination rate [35]. A potential drawback is interface band gap narrowing, which can decrease E_A if interface recombination dominates. The more Zn diffusion into CdS, the larger the upward CBM shift of CdS, which also contributes to increasing the CBO. However, the beneficial effect of Zn diffusion must be balanced against the likely series resistance increase due to ZnS segregation [4, 87, 96], as discussed in Sec. 9.

We then conclude that interdiffusion can actually be *beneficial* in CZTS solar cells as it may increase an originally cliff-like CBO to a spike-like CBO within the optimal range for photovoltaics. Additionally, interdiffusion improves lattice matching at the CZTS/CdS interface (Sec. 10), which may decrease the interface defect density and thus the interface recombination velocities. This can explain the success of solar cells based on the CZTS/$Zn_{1-x}Cd_xS$ heterojunction [94], where Zn was deliberately alloyed with Cd to increase the CBO. Assuming no simultaneous detrimental effects, Cd and Zn interdiffusion should therefore be promoted in CZTS/CdS solar cells.

12.2. The case of CZTSe

The CBOs measured at the CZTSe/CdS interface (Fig. 3) are close to the upper limit of the optimal range for photovoltaics. Unlike the case of CZTS, interdiffusion may then be detrimental for solar cell performance. Cd interdiffusion is expected to increase the CBO as in CTZS solar cell, due to the upward CBM shift in CZTS. Zn and Se interdiffusion may not have any significant effect on the CBO if Se interdiffusion is predominant, as in Fig. 11. However, the CBO may increase further in the case of dominant Zn interdiffusion, as demonstrated experimentally in [19].

We then conclude that interdiffusion is most likely to be *detrimental* in CZTSe solar cells, since it is expected to increase a CBO that is already close to the upper limit of its optimal range. A CBO that is larger than the optimal range is, however, easier to diagnose than a CBO below the optimal range because of its peculiar effects on the illuminated current-voltage (JV) curve of the solar cell, i.e., a kink or nearly full current blockage [8, 19].

13. Conclusion

We have argued that the large deviation in the CBO measured at the CZTS(e)/CdS interface by different workers is likely to be caused both by genuine process-dependent variations and by errors in its experimental determination. Real CBO variations can be due to many different physical and chemical mechanisms that influence the band edge positions of CZTS(e) and CdS at the heterointerface, at bare surfaces, or in the bulk. Those mechanisms have been analyzed in this article. Fermi level pinning (which tends to decrease the CBO) and chemical interdiffusion (which tends to increase the CBO) have been identified as crucial. Further variations may be caused by etching of the absorber and by quantum confinement in the CdS seed layer. There also exist some mechanisms that do not modify the average CBO across the interface but may cause lateral inhomogeneity in the CBO in the interface plane. Polar interfaces, band gap fluctuations, local formation of an epitaxial interface, and phase inhomogeneity in CdS have been identified as such. A summary of the impact of those mechanisms on the VBO and CBO of the CZTS(e)/CdS interface is presented in Table 3.

Five photoemission-based measurement approaches have been analyzed to point out possible limitations in the CBO values determined with each approach. The influence of Fermi level pinning on the CBO should be captured correctly by all types of measurements except for the flat-band VB method, where there is a possibility of Fermi level de-pinning upon optical pumping. This would lead to overestimation of both the CBO and interface band bending, which may explain some unusually large values of the CBO and of band bending reported before. On the other hand, the influence of interdiffusion is difficult to resolve completely by most measurement approaches. Therefore, the measured CBO of CZTS/CdS interfaces (CZTSe/CdS interfaces) may be systematically underestimated (overestimated) if substantial interdiffusion occurs. A summary of other possible errors related to the mechanisms

discussed in this paper is presented in Table 3. Among the analyzed measurement approaches, the direct CB approach is the only one that can (in principle) fully resolve band edge modifications at the interface that affect the CBO, including the effects of interdiffusion. However, the risk of altering conduction band features by ion beam etching may limit the applicability of the approach. The direct VB approach combined with a depth-resolved measurement of band gaps by an optical technique could yield accurate results, even though this is yet to be demonstrated.

Finally, CdS is often considered inadequate as a buffer layer for pure-sulfide CZTS due to many reports of a cliff-like CBO. However, obtaining an optimal spike-like CBO at CZTS/CdS heterojunctions seems to be both *possible* and *necessary* for high-efficiency CZTS/CdS solar cells. In fact, a rough correlation could be established between the CBO measured at the CZTS/CdS interface by different groups and their corresponding solar cell efficiency: lower-efficiency cells often have a large "cliff-like" offset, whereas most high-efficiency cells have a small "spike-like" offset or nearly flat offset. Since the CBO of CZTS/CdS interfaces can be underestimated upon substantial interdiffusion, it is possible that the CBO is even higher than what has been measured. Control of interdiffusion in CZTS/CdS solar cells can be a powerful way to improve the interface properties by two simultaneous effects: (i) increase of the CBO towards the optimal range for maximum efficiency, and (ii) reduction of the lattice mismatch between CZTS and CdS. There can of course be other valid reasons (Cd toxicity, insufficient passivation of surface states) to replace CdS by another material. Nevertheless, this work has shown that an optimal CBO at the CZTS/CdS interface can be reached experimentally without obvious detrimental side effects.

Acknowledgments

This work was supported by a research grant (9455) from Villum Fonden and from the Danish Council for Strategic Research (12-132644).

References

[1] A. Polman, M. Knight, E. C. Garnett, B. Ehrler, W. C. Sinke, Photovoltaic materials: Present efficiencies and future challenges, Science 352 (6283) (2016) aad4424. doi:10.1126/science.aad4424.

[2] W. Wang, M. T. Winkler, O. Gunawan, T. Gokmen, T. K. Todorov, Y. Zhu, D. B. Mitzi, Device Characteristics of CZTSSe Thin-Film Solar Cells with 12.6% Efficiency, Advanced Energy Materials 4 (7) (2013) 1301465. doi:10.1002/aenm.201301465.

[3] S. Tajima, M. Umehara, M. Hasegawa, T. Mise, T. Itoh, Cu_2ZnSnS_4 photovoltaic cell with improved efficiency fabricated by high-temperature annealing after CdS buffer-layer deposition, Progress in Photovoltaics: Research and Applicationsdoi:10.1002/pip.2837.

[4] A. Redinger, M. Mousel, M. H. Wolter, N. Valle, S. Siebentritt, Influence of S/Se ratio on series resistance and on dominant recombination pathway in $Cu_2ZnSn(S,Se)_4$ thin film solar cells, Thin Solid Films 535 (2013) 291–295. doi:10.1016/j.tsf.2012.11.111.

[5] T. Gokmen, O. Gunawan, D. B. Mitzi, Semi-empirical device model for $Cu_2ZnSn(S,Se)_4$ solar cells, Applied Physics Letters 105 (3) (2014) 033903. doi:10.1063/1.4890844.

[6] S. Tajima, T. Itoh, H. Hazama, K. Ohishi, R. Asahi, Improvement of the open-circuit voltage of Cu_2ZnSnS_4 solar cells using a two-layer structure, Applied Physics Express 8 (8) (2015) 082302. doi:10.7567/APEX.8.082302.

[7] K. Wang, O. Gunawan, T. Todorov, B. Shin, S. J. Chey, N. A. Bojarczuk, D. Mitzi, S. Guha, Thermally evaporated Cu_2ZnSnS_4 solar cells, Applied Physics Letters 97 (14) (2010) 143508. doi:10.1063/1.3499284.

[8] T. Ericson, J. J. Scragg, A. Hultqvist, J. T. Watjen, P. Szaniawski, T. Torndahl, C. Platzer-Björkman, Zn(O,S) Buffer Layers and Thickness Variations of CdS Buffer for Cu_2ZnSnS_4 Solar Cells, IEEE Journal of Photovoltaics 4 (1) (2014) 465–469. doi:10.1109/JPHOTOV.2013.2283058.

[9] R. Scheer, Activation energy of heterojunction diode currents in the limit of interface recombination, Journal of Applied Physics 105 (10) (2009) 104505. doi:10.1063/1.3126523.

[10] M. Baer, B.-A. Schubert, B. Marsen, R. G. Wilks, S. Pookpanratana, M. Blum, S. Krause, T. Unold, W. Yang, L. Weinhardt, C. Heske, H.-W. Schock, Cliff-like conduction band offset and KCN-induced recombination barrier enhancement at the CdS/Cu_2ZnSnS_4 thin-film solar cell heterojunction, Applied Physics Letters 99 (22) (2011) 222105. doi:10.1063/1.3663327.

[11] S. Tajima, K. Kataoka, N. Takahashi, Y. Kimoto, T. Fukano, M. Hasegawa, H. Hazama, Direct measurement of band offset at the interface between CdS and Cu_2ZnSnS_4 using hard X-ray photoelectron spectroscopy, Applied Physics Letters 103 (24) (2013) 243906. doi:10.1063/1.4850235.

[12] N. Terada, S. Yoshimoto, K. Chochi, T. Fukuyama, M. Mitsunaga, H. Tampo, H. Shibata, K. Matsubara, S. Niki, N. Sakai, T. Katou, H. Sugimoto, Characterization of electronic structure of $Cu_2ZnSn(S_xSe_{1-x})_4$ absorber layer and CdS/$Cu_2ZnSn(S_xSe_{1-x})_4$ interfaces by in-situ photoemission and inverse photoemission spectroscopies, Thin Solid Films 582 (2015) 166–170. doi:10.1016/j.tsf.2014.09.037.

[13] C. Yan, F. Liu, N. Song, B. K. Ng, J. A. Stride, A. Tadich, X. Hao, Band alignments of different buffer layers (CdS, Zn(O,S), and In_2S_3) on Cu_2ZnSnS_4, Applied Physics Letters 104 (17) (2014) 173901. doi:10.1063/1.4873715.

[14] J. Li, Q. Du, W. Liu, G. Jiang, X. Feng, W. Zhang, J. Zhu, C. Zhu, The band offset at CdS/Cu_2ZnSnS_4 heterojunction interface, Electronic Materials Letters 8 (4) (2012) 365–367. doi:10.1007/s13391-012-2023-0.

[15] A. Santoni, F. Biccari, C. Malerba, M. Valentini, R. Chierchia, A. Mittiga, Valence band offset at the CdS/Cu_2ZnSnS_4 interface probed by x-ray photoelectron spectroscopy, Journal of Physics D: Applied Physics 46 (17) (2013) 175101. doi:10.1088/0022-3727/46/17/175101.

[16] S. Huang, W. Luo, Z. Zou, Band positions and photoelectrochemical properties of Cu_2ZnSnS_4 thin films by the ultrasonic spray pyrolysis method, Journal of Physics D: Applied Physics 46 (23) (2013) 235108. doi:10.1088/0022-3727/46/23/235108.

[17] R. Haight, A. Barkhouse, O. Gunawan, B. Shin, M. Copel, M. Hopstaken, D. B. Mitzi, Band alignment at the $Cu_2ZnSn(S_xSe_{1-x})_4$/CdS interface, Applied Physics Letters 98 (25) (2011) 253502. doi:10.1063/1.3600776.

[18] J. Li, M. Wei, Q. Du, W. Liu, G. Jiang, C. Zhu, The band alignment at CdS/$Cu_2ZnSnSe_4$ heterojunction interface, Surface and Interface Analysis 45 (2) (2013) 682–684. doi:10.1002/sia.5095.

[19] T. Kato, H. Hiroi, N. Sakai, H. Sugimoto, Buffer/Absorber Interface Study on Cu_2ZnSnS_4 and $Cu_2ZnSnSe_4$ Based Solar Cells: Band Alignment and Its Impact on the Solar Cell Performance, in: 28th European Photovoltaic Solar Energy Conference and Exhibition, WIP, 2013, pp. 2125–2127. doi:10.4229/28thEUPVSEC2013-3AO.5.1.

[20] H. Hiroi, N. Sakai, T. Kato, H. Sugimoto, High voltage Cu_2ZnSnS_4 submodules by hybrid buffer layer, in: 2013 IEEE 39th Photovoltaic Specialists Conference (PVSC), IEEE, 2013, pp. 0863–0866. doi:10.1109/PVSC.2013.6744281.

[21] Z.-Y. Dong, Y.-F. Li, B. Yao, Z.-H. Ding, G. Yang, R. Deng, X. Fang, Z.-P. Wei, L. Liu, An experimental and first-principles study on band alignments at interfaces of Cu_2ZnSnS_4/CdS/ZnO heterojunctions, Journal of Physics D: Applied Physics 47 (7) (2014) 075304. doi:10.1088/0022-3727/47/7/075304.

[22] M. Than Htay, R. Fujimura, R. Hasuike, K. Takei, N. Momose,

Y. Hashimoto, K. Ito, Effect of ultrasonically generated water vapor treatment on the Cu_2ZnSnS_4/CdS heterojunction-based photovoltaic cells, Solar Energy Materials and Solar Cells 157 (2016) 765–776. doi:10.1016/j.solmat.2016.07.014.

[23] H.-J. Chen, S.-W. Fu, S.-H. Wu, T.-C. Tsai, H.-T. Wu, C.-F. Shih, Structural and photoelectron spectroscopic studies of band alignment at the Cu_2ZnSnS_4 /CdS heterojunction with slight Ni doping in Cu_2ZnSnS_4, Journal of Physics D: Applied Physics 49 (33) (2016) 335102. doi:10.1088/0022-3727/49/33/335102.

[24] K. Kataoka, S. Tajima, M. Umehara, N. Takahashi, N. Isomura, K. Kitazumi, Y. Kimoto, Band slope in CdS layer of ZnO:Ga/CdS/Cu_2ZnSnS_4 photovoltaic cells revealed by hard X-ray photoelectron spectroscopy, Applied Physics Letters 109 (20) (2016) 203902. doi:10.1063/1.4967979.

[25] K. Sardashti, R. Haight, T. Gokmen, W. Wang, L.-Y. Chang, D. B. Mitzi, A. C. Kummel, Impact of Nanoscale Elemental Distribution in High-Performance Kesterite Solar Cells, Advanced Energy Materials 5 (10) (2015) 1402180. doi:10.1002/aenm.201402180.

[26] Y. Udaka, S. Takaki, K. Isowaki, T. Nagai, K. M. Kim, S. Kim, H. Tampo, H. Shibata, K. Matsubara, S. Niki, N. Sakai, T. Kato, H. Sugimoto, N. Terada, Electronic structure of $Cu_2ZnSn(S_xSe_{1-x})_4$ surface and CdS/$Cu_2ZnSn(S_xSe_{1-x})_4$ interface, physica status solidi (c)doi:10.1002/PSSC.201600178.

[27] M. Palsgaard, A. Crovetto, T. Gunst, T. Markussen, O. Hansen, K. Stokbro, M. Brandbyge, Semiconductor band alignment from first principles: A new nonequilibrium Green's function method applied to the CZTSe/CdS interface for photovoltaics, in: 2016 International Conference on Simulation of Semiconductor Processes and Devices (SISPAD), IEEE, Nuremberg, Germany, 2016, pp. 377–380. doi:10.1109/SISPAD.2016.7605225.

[28] S. Chen, J. Yang, X. Gong, A. Walsh, S. Wei, Intrinsic point defects and complexes in the quaternary kesterite semiconductor Cu_2ZnSnS_4, Physical Review B 81 (24) (2010) 245204.

[29] S. Chen, A. Walsh, J.-H. Yang, X. G. Gong, L. Sun, P.-X. Yang, J.-H. Chu, S.-H. Wei, Compositional dependence of structural and electronic properties of $Cu_2ZnSn(S,Se)_4$ alloys for thin film solar cells, Physical Review B 83 (12) (2011) 125201. doi:10.1103/PhysRevB.83.125201.

[30] A. Nagoya, R. Asahi, G. Kresse, First-principles study of Cu_2ZnSnS_4 and the related band offsets for photovoltaic applications., Journal of physics. Condensed matter : an Institute of Physics journal 23 (40) (2011) 404203. doi:10.1088/0953-8984/23/40/404203.

[31] W. Bao, M. Ichimura, Prediction of the Band Offsets at the CdS/Cu_2ZnSnS_4 Interface Based on the First-Principles Calculation, Japanese Journal of Applied Physics 51 (10S) (2012) 10NC31. doi:10.1143/JJAP.51.10NC31.

[32] W. Bao, M. Ichimura, First-Principles Study on Influences of Crystal Structure and Orientation on Band Offsets at the CdS/Cu_2ZnSnS_4 Interface, International Journal of Photoenergy 2012 (Article ID 619812) (2012) 5 pages.

[33] A. Crovetto, M. Palsgaard, T. Gunst, T. Markussen, K. Stokbro, M. Brandbyge, O. Hansen, Interface band gap narrowing behind open circuit voltage losses in Cu_2ZnSnS_4 solar cells, Applied Physics Letters 110 (8) (2017) 083903. doi:10.1063/1.4976830.

[34] T. Minemoto, T. Matsui, H. Takakura, Y. Hamakawa, T. Negami, Y. Hashimoto, T. Uenoyama, M. Kitagawa, Theoretical analysis of the effect of conduction band offset of window/CIS layers on performance of CIS solar cells using device simulation, Solar Energy Materials and Solar Cells 67 (1) (2001) 83–88.

[35] M. Gloeckler, J. Sites, Efficiency limitations for wide-band-gap chalcopyrite solar cells, Thin Solid Films 480-481 (2005) 241–245. doi:10.1016/j.tsf.2004.11.018.

[36] J. Robertson, Band offsets, Schottky barrier heights, and their effects on electronic devices, Journal of Vacuum Science & Technology A: Vacuum, Surfaces, and Films 31 (5) (2013) 050821. doi:10.1116/1.4818426.

[37] A. Klein, Energy band alignment in chalcogenide thin film solar cells from photoelectron spectroscopy, Journal of Physics: Condensed Matter 27 (13) (2015) 134201. doi:10.1088/0953-8984/27/13/134201.

[38] W. Monch, Electronic Properties of Semiconductor Interfaces, Springer, Heidelberg, 2004.

[39] J. Tersoff, The theory of heterojunction band lineups, in: G. Capasso, G. Margaritondo (Eds.), Heterojunction band discontinuities: Physics and device applications, North-Holland, Amsterdam, 1987, Ch. 1.

[40] W. R. L. Lambrecht, B. Segall, Interface-bond-polarity model for semiconductor heterojunction band offsets, Physical Review B 41 (5) (1990) 2832–2848. doi:10.1103/PhysRevB.41.2832.

[41] W. Mönch, Role of virtual gap states and defects in metal-semiconductor contacts, Physical Review Letters 58 (12) (1987) 1260–1263. doi:10.1103/PhysRevLett.58.1260.

[42] R. Scheer, H.-W. Schock, Chalcogenide Photovoltaics, Wiley-VCH Verlag GmbH & Co. KGaA, Weinheim, Germany, 2011. doi:10.1002/9783527633708.

[43] S. Tanuma, C. J. Powell, D. R. Penn, Calculations of electron inelastic mean free paths. IX. Data for 41 elemental solids over the 50 eV to 30 keV range, Surface and Interface Analysis 43 (3) (2011) 689–713. doi:10.1002/sia.3522.

[44] A. Crovetto, A. Cazzaniga, R. B. Ettlinger, J. Schou, O. Hansen, Optical properties and surface characterization of pulsed laser-deposited Cu_2ZnSnS_4 by spectroscopic ellipsometry, Thin Solid Films 582 (2015) 203–207. doi:10.1016/j.tsf.2014.11.075.

[45] Y. Hinuma, A. Grüneis, G. Kresse, F. Oba, Band alignment of semiconductors from density-functional theory and many-body perturbation theory, Physical Review B 90 (15) (2014) 155405. doi:10.1103/PhysRevB.90.155405.

[46] S.-H. Wei, A. Zunger, Calculated natural band offsets of all IIVI and IIIV semiconductors: Chemical trends and the role of cation d orbitals, Applied Physics Letters 72 (16) (1998) 2011. doi:10.1063/1.121249.

[47] A. Alkauskas, P. Broqvist, F. Devynck, A. Pasquarello, Band Offsets at Semiconductor-Oxide Interfaces from Hybrid Density-Functional Calculations, Physical Review Letters 101 (10) (2008) 106802. doi:10.1103/PhysRevLett.101.106802.

[48] Y.-H. Li, A. Walsh, S. Chen, W.-J. Yin, J.-H. Yang, J. Li, J. L. F. Da Silva, X. G. Gong, S.-H. Wei, Revised ab initio natural band offsets of all group IV, II-VI, and III-V semiconductors, Applied Physics Letters 94 (21) (2009) 212109. doi:10.1063/1.3143626.

[49] J. P. Perdew, K. Burke, M. Ernzerhof, Generalized Gradient Approximation Made Simple, Physical Review Letters 77 (18) (1996) 3865–3868. doi:10.1103/PhysRevLett.77.3865.

[50] V. I. Anisimov, J. Zaanen, O. K. Andersen, Band theory and Mott insulators: Hubbard U instead of Stoner I, Physical Review B 44 (3) (1991) 943–954. doi:10.1103/PhysRevB.44.943.

[51] J. Heyd, G. E. Scuseria, M. Ernzerhof, Hybrid functionals based on a screened Coulomb potential, The Journal of Chemical Physics 118 (18) (2003) 8207. doi:10.1063/1.1564060.

[52] M. Bär, B.-A. Schubert, B. Marsen, S. Schorr, R. G. Wilks, L. Weinhardt, S. Pookpanratana, M. Blum, S. Krause, Y. Zhang, W. Yang, T. Unold, C. Heske, H.-W. Schock, Electronic structure of Cu_2ZnSnS_4 probed by soft x-ray emission and absorption spectroscopy, Physical Review B 84 (3) (2011) 035308. doi:10.1103/PhysRevB.84.035308.

[53] D. Lim, R. Haight, In situ photovoltage measurements using femtosecond pump-probe photoelectron spectroscopy and its application to metal-HfO_2Si structures, Journal of Vacuum Science & Technology A: Vacuum, Surfaces, and Films 23 (6) (2005) 1698. doi:10.1116/1.2083909.

[54] B. Shin, O. Gunawan, Y. Zhu, N. A. Bojarczuk, S. J. Chey, S. Guha, Thin film solar cell with 8.4% power conversion efficiency using an earth-abundant Cu_2ZnSnS_4 absorber, Progress in Photovoltaics: Research and Applications 21 (1) (2011) 72–76. doi:10.1002/pip.1174.

[55] B.-A. Schubert, B. Marsen, S. Cinque, T. Unold, R. Klenk, S. Schorr, H.-W. Schock, Cu_2ZnSnS_4 thin film solar cells by fast coevaporation, Progress in Photovoltaics: Research and Applications 19 (1) (2011) 93–96. doi:10.1002/pip.976.

[56] C. Malerba, Cu_2ZnSnS_4 thin films and solar cells: material and device characterization, Phd thesis, University of Trento (2014).

[57] M. Burgelman, P. Nollet, S. Degrave, Modelling polycrystalline semiconductor solar cells, Thin Solid Films 361-362 (2000) 527–532. doi:10.1016/S0040-6090(99)00825-1.

[58] S. Siol, J. C. Hellmann, S. D. Tilley, M. Graetzel, J. Morasch, J. Deuermeier, W. Jaegermann, A. Klein, Band Alignment Engineering at Cu_2O/ZnO Heterointerfaces, ACS Applied Materials & Interfaces 8 (33) (2016) 21824–21831. doi:10.1021/acsami.6b07325.

[59] S. B. Zhang, S.-H. Wei, A. Zunger, A phenomenological model for systematization and prediction of doping limits in IIVI and

IIIIVI$_2$ compounds, Journal of Applied Physics 83 (6) (1998) 3192. doi:10.1063/1.367120.

[60] R. Haight, X. Shao, W. Wang, D. B. Mitzi, Electronic and elemental properties of the $Cu_2ZnSn(S,Se)_4$ surface and grain boundaries, Applied Physics Letters 104 (3) (2014) 033902. doi:10.1063/1.4862791.

[61] H. Du, M. J. Romero, I. Repins, G. Teeter, R. Noufi, M. M. Al-Jassim, Nanoscale measurements of the surface photovoltage in $Cu(In,Ga)Se_2$, Cu_2ZnSnS_4, and $Cu_2ZnSnSe_4$ thin films: The role of the surface electronics on the efficiency of solar cells, in: 2011 37th IEEE Photovoltaic Specialists Conference, IEEE, 2011, pp. 001983–001986. doi:10.1109/PVSC.2011.6186342.

[62] W. A. Harrison, E. A. Kraut, J. R. Waldrop, R. W. Grant, Polar heterojunction interfaces, Physical Review B 18 (8) (1978) 4402–4410. doi:10.1103/PhysRevB.18.4402.

[63] A. Polizzotti, I. L. Repins, R. Noufi, S.-H. Wei, D. B. Mitzi, The state and future prospects of kesterite photovoltaics, Energy & Environmental Science 6 (11) (2013) 3171–3182. doi:10.1039/c3ee41781f.

[64] P. W. Tasker, The stability of ionic crystal surfaces, Journal of Physics C: Solid State Physics 12 (22) (1979) 4977–4984. doi:10.1088/0022-3719/12/22/036.

[65] R. W. Grant, J. R. Waldrop, E. A. Kraut, Observation of the Orientation Dependence of Interface Dipole Energies in Ge-GaAs, Physical Review Letters 40 (10) (1978) 656–659. doi:10.1103/PhysRevLett.40.656.

[66] R. Nicolini, L. Vanzetti, G. Mula, G. Bratina, L. Sorba, A. Franciosi, M. Peressi, S. Baroni, R. Resta, A. Baldereschi, J. E. Angelo, W. W. Gerberich, Local interface composition and band discontinuities in heterovalent heterostructures, Physical Review Letters 72 (2) (1994) 294–297. doi:10.1103/PhysRevLett.72.294.

[67] A. Crovetto, C. Yan, B. Iandolo, F. Zhou, J. Stride, J. Schou, X. Hao, O. Hansen, Lattice-matched Cu_2ZnSnS_4/CeO_2 solar cell with open circuit voltage boost, Applied Physics Letters 109 (23) (2016) 233904. doi:10.1063/1.4971779.

[68] F. Liu, C. Yan, J. Huang, K. Sun, F. Zhou, J. A. Stride, M. A. Green, X. Hao, Nanoscale Microstructure and Chemistry of Cu_2ZnSnS_4/CdS Interface in Kesterite Cu_2ZnSnS_4 Solar Cells, Advanced Energy Materials 6 (15) (2016) 1600706. doi:10.1002/aenm.201600706.

[69] H. Kroemer, Heterostructure devices: A device physicist looks at interfaces, Surface Science 132 (1) (1983) 543–576. doi:10.1016/0039-6028(83)90561-7.

[70] J. Jaffe, A. Zunger, Defect-induced nonpolar-to-polar transition at the surface of chalcopyrite semiconductors, Physical Review B 64 (24) (2001) 241304. doi:10.1103/PhysRevB.64.241304.

[71] P. Xu, S. Chen, B. Huang, H. J. Xiang, X.-G. Gong, S.-H. Wei, Stability and electronic structure of Cu_2ZnSnS_4 surfaces: First-principles study, Physical Review B 88 (4) (2013) 045427. doi:10.1103/PhysRevB.88.045427.

[72] D. B. Mitzi, O. Gunawan, T. K. Todorov, K. Wang, S. Guha, The path towards a high-performance solution-processed kesterite solar cell, Solar Energy Materials and Solar Cells 95 (6) (2011) 1421–1436. doi:10.1016/j.solmat.2010.11.028.

[73] J. J. S. Scragg, L. Choubrac, A. Lafond, T. Ericson, C. Platzer-Björkman, A low-temperature order-disorder transition in Cu_2ZnSnS_4 thin films, Applied Physics Letters 104 (4) (2014) 041911. doi:10.1063/1.4863685.

[74] G. Rey, A. Redinger, J. Sendler, T. P. Weiss, M. Thevenin, M. Guennou, B. El Adib, S. Siebentritt, The band gap of $Cu_2ZnSnSe_4$: Effect of order-disorder, Applied Physics Letters 105 (11) (2014) 112106. doi:10.1063/1.4896315.

[75] M. Valentini, C. Malerba, F. Menchini, D. Tedeschi, A. Polimeni, M. Capizzi, A. Mittiga, Effect of the order-disorder transition on the optical properties of Cu_2ZnSnS_4, Applied Physics Letters 108 (21) (2016) 211909. doi:10.1063/1.4952973.

[76] S. Chen, A. Walsh, X.-G. Gong, S.-H. Wei, Classification of Lattice Defects in the Kesterite Cu_2ZnSnS_4 and $Cu_2ZnSnSe_4$ Earth-Abundant Solar Cell Absorbers, Advanced Materials 25 (11) (2013) 1522–1539. doi:10.1002/adma.201203146.

[77] S. Siebentritt, G. Rey, A. Finger, D. Regesch, J. Sendler, T. P. Weiss, T. Bertram, What is the bandgap of kesterite?, Solar Energy Materials and Solar Cellsdoi:10.1016/j.solmat.2015.10.017.

[78] Y. S. Lee, T. Gershon, O. Gunawan, T. K. Todorov, T. Gokmen, Y. Virgus, S. Guha, $Cu_2ZnSnSe_4$ Thin-Film Solar Cells by Thermal Co-evaporation with 11.6% Efficiency and Improved Minority Carrier Diffusion Length, Advanced Energy Materials 5 (7) (2015) 1401372. doi:10.1002/aenm.201401372.

[79] G. Hodes, Chemical solution deposition of semiconductor films, Marcel Dekker, New York, Basel, 2002.

[80] M. Murayama, T. Nakayama, Chemical trend of band offsets at wurtzite/zinc-blende heterocrystalline semiconductor interfaces, Physical Review B 49 (7) (1994) 4710–4724. doi:10.1103/PhysRevB.49.4710.

[81] K. I. Kang, B. P. McGinnis, Sandalphon, Y. Z. Hu, S. W. Koch, N. Peyghambarian, A. Mysyrowicz, L. C. Liu, S. H. Risbud, Confinement-induced valence-band mixing in CdS quantum dots observed by two-photon spectroscopy, Physical Review B 45 (7) (1992) 3465–3468. doi:10.1103/PhysRevB.45.3465.

[82] J. Lindahl, J. Keller, O. Donzel-Gargand, P. Szaniawski, M. Edoff, T. Törndahl, Deposition temperature induced conduction band changes in zinc tin oxide buffer layers for $Cu(In,Ga)Se_2$ solar cells, Solar Energy Materials and Solar Cells 144 (2016) 684–690. doi:10.1016/j.solmat.2015.09.048.

[83] Y. Wang, N. Herron, Quantum size effects on the exciton energy of CdS clusters, Physical Review B 42 (11) (1990) 7253–7255. doi:10.1103/PhysRevB.42.7253.

[84] S. Tajima, H. Katagiri, K. Jimbo, N. Sugimoto, T. Fukano, Temperature Dependence of Cu_2ZnSnS_4 Photovoltaic Cell Properties, Applied Physics Express 5 (8) (2012) 082302. doi:10.1143/APEX.5.082302.

[85] F. Liu, Y. Lai, J. Liu, B. Wang, S. Kuang, Z. Zhang, J. Li, Y. Liu, Characterization of chemical bath deposited CdS thin films at different deposition temperature, Journal of Alloys and Compounds 493 (1) (2010) 305–308. doi:10.1016/j.jallcom.2009.12.088.

[86] C. G. Van de Walle, L. H. Yang, Band discontinuities at heterojunctions between crystalline and amorphous silicon, Journal of Vacuum Science & Technology B: Microelectronics and Nanometer Structures 13 (4) (1995) 1635. doi:10.1116/1.587870.

[87] S. Tajima, R. Asahi, D. Isheim, D. N. Seidman, T. Itoh, M. Hasegawa, K. Ohishi, Atom-probe tomographic study of interfaces of Cu_2ZnSnS_4 photovoltaic cells, Applied Physics Letters 105 (9) (2014) 093901. doi:10.1063/1.4894858.

[88] Z. Su, J. M. R. Tan, X. Li, X. Zeng, S. K. Batabyal, L. H. Wong, Cation Substitution of Solution-Processed Cu_2ZnSnS_4 Thin Film Solar Cell with over 9% Efficiency, Advanced Energy Materials 5 (19) (2015) 1500682. doi:10.1002/aenm.201500682.

[89] C. Persson, A. Zunger, Anomalous Grain Boundary Physics in Polycrystalline $CuInSe_2$: The Existence of a Hole Barrier, Physical Review Letters 91 (26) (2003) 266401. doi:10.1103/PhysRevLett.91.266401.

[90] S. López-Marino, Y. Sánchez, M. Placidi, A. Fairbrother, M. Espindola-Rodríguez, X. Fontané, V. Izquierdo-Roca, J. López-García, L. Calvo-Barrio, A. Pérez-Rodríguez, E. Saucedo, ZnSe etching of Zn-rich $Cu_2ZnSnSe_4$: an oxidation route for improved solar-cell efficiency., Chemistry (Weinheim an der Bergstrasse, Germany) 19 (44) (2013) 14814–22. doi:10.1002/chem.201302589.

[91] W. Li, J. Chen, C. Yan, X. Hao, The effect of ZnS segregation on Zn-rich CZTS thin film solar cells, Journal of Alloys and Compounds 632 (2015) 178–184. doi:10.1016/j.jallcom.2015.01.205.

[92] A. Fairbrother, E. García-Hemme, V. Izquierdo-Roca, X. Fontané, F. A. Pulgarín-Agudelo, O. Vigil-Galán, A. Pérez-Rodríguez, E. Saucedo, Development of a selective chemical etch to improve the conversion efficiency of Zn-rich Cu_2ZnSnS_4 solar cells., Journal of the American Chemical Society 134 (19) (2012) 8018–21. doi:10.1021/ja301373e.

[93] C. Yan, F. Liu, K. Sun, N. Song, J. A. Stride, F. Zhou, X. Hao, M. Green, Boosting the efficiency of pure sulfide CZTS solar cells using the In/Cd-based hybrid buffers, Solar Energy Materials and Solar Cells 144 (2016) 700–706. doi:10.1016/j.solmat.2015.10.019.

[94] K. Sun, C. Yan, F. Liu, J. Huang, F. Zhou, J. A. Stride, M. Green, X. Hao, Over 9% Efficient Kesterite Cu_2ZnSnS_4 Solar Cell Fabricated by Using $Zn_{1-x}Cd_xS$ Buffer Layer, Advanced Energy Materials 6 (12) (2016) 1600046. doi:10.1002/aenm.201600046.

[95] M. Bar, B.-A. Schubert, B. Marsen, S. Krause, S. Pookpanratana, T. Unold, L. Weinhardt, C. Heske, H.-W. Schock, Impact of KCN etching on the chemical and electronic surface structure of Cu_2ZnSnS_4 thin-film solar cell absorbers, Applied Physics Letters 99 (15) (2011) 152111. doi:10.1063/1.3650717.

[96] N. Sakai, H. Hiroi, H. Sugimoto, Development of Cd-free buffer

layer for Cu_2ZnSnS_4 thin-film solar cells, in: 2011 37th IEEE Photovoltaic Specialists Conference, IEEE, 2011, pp. 003654–003657. doi:10.1109/PVSC.2011.6185941.

[97] K. F. Tai, O. Gunawan, M. Kuwahara, S. Chen, S. G. Mhaisalkar, C. H. A. Huan, D. B. Mitzi, Fill Factor Losses in $Cu_2ZnSn(S_xSe_{1-x})_4$ Solar Cells: Insights from Physical and Electrical Characterization of Devices and Exfoliated Films, Advanced Energy Materials 6 (3) (2016) 1501609. doi:10.1002/aenm.201501609.

[98] S. S. Wilson, J. P. Bosco, Y. Tolstova, D. O. Scanlon, G. W. Watson, H. A. Atwater, Interface stoichiometry control to improve device voltage and modify band alignment in ZnO/Cu_2O heterojunction solar cells, Energy Environ. Sci. 7 (11) (2014) 3606–3610. doi:10.1039/C4EE01956C.

[99] C. Heske, D. Eich, R. Fink, E. Umbach, T. van Buuren, C. Bostedt, L. J. Terminello, S. Kakar, M. M. Grush, T. A. Callcott, F. J. Himpsel, D. L. Ederer, R. C. C. Perera, W. Riedl, F. Karg, Observation of intermixing at the buried CdS/Cu(In,Ga)Se_2 thin film solar cell heterojunction, Applied Physics Letters 74 (10) (1999) 1451. doi:10.1063/1.123578.

[100] T. Nakada, Nano-structural investigations on Cd-doping into Cu(In,Ga)Se_2 thin films by chemical bath deposition process, Thin Solid Films 361 (2000) 346–352. doi:10.1016/S0040-6090(99)00767-1.

[101] M. Morkel, L. Weinhardt, B. Lohmueller, C. Heske, E. Umbach, W. Riedl, S. Zweigart, F. Karg, Flat conduction-band alignment at the CdS/$CuInSe_2$ thin-film solar-cell heterojunction, Applied Physics Letters 79 (27) (2001) 4482. doi:10.1063/1.1428408.

[102] J. P. Enríquez, E. Gómez Barojas, R. Silva González, U. Pal, S and Te inter-diffusion in CdTe/CdS hetero junction, Solar Energy Materials and Solar Cells 91 (15) (2007) 1392–1397. doi:10.1016/j.solmat.2007.05.008.

[103] J. Kim, S. Park, S. Ryu, J. Oh, B. Shin, Improving the open-circuit voltage of $Cu_2ZnSnSe_4$ thin film solar cells via interface passivation, Progress in Photovoltaics: Research and Applications 25 (4) (2017) 308–317. doi:10.1002/pip.2864.

[104] T. Maeda, S. Nakamura, T. Wada, First-Principles Study on Cd Doping in Cu_2ZnSnS_4 and $Cu_2ZnSnSe_4$, Japanese Journal of Applied Physics 51 (10S) (2012) 10NC11. doi:10.1143/JJAP.51.10NC11.

[105] Z.-Y. Xiao, Y.-F. Li, B. Yao, R. Deng, Z.-H. Ding, T. Wu, G. Yang, C.-R. Li, Z.-Y. Dong, L. Liu, L.-G. Zhang, H.-F. Zhao, Bandgap engineering of $Cu_2Cd_xZn_{1-x}SnS_4$ alloy for photovoltaic applications: A complementary experimental and first-principles study, Journal of Applied Physics 114 (18) (2013) 183506. doi:10.1063/1.4829457.

[106] A. Crovetto, R. Chen, R. B. Ettlinger, A. C. Cazzaniga, J. Schou, C. Persson, O. Hansen, Dielectric function and double absorption onset of monoclinic Cu_2SnS_3: Origin of experimental features explained by first-principles calculations, Solar Energy Materials and Solar Cells 154 (2016) 121–129. doi:10.1016/j.solmat.2016.04.028.